Evaluation of agriculture land transformations with socio-economic influences on wheat demand and supply for food sustainability

Danish Raza, Hong Shu, Muhsan Ehsan, Hong Fan, Kamal Abdelrahman, Hasnat Aslam, Abdul Quddoos, Rana Waqar Aslam, Majid Nazeer, Mohammed S. Fnais & Azeem Sardar

Published online: 07 Jan 2025.

Submit your article to this journal ☑

Article views: 1006

View related articles ☑

View Crossmark data ☑

Citing articles: 2 View citing articles ☑

co*gent

SOIL & CROP SCIENCES | RESEARCH ARTICLE

Evaluation of agriculture land transformations with socio-economic influences on wheat demand and supply for food sustainability

Danish Raza[a] [ID], Hong Shu[a], Muhsan Ehsan[b], Hong Fan[a], Kamal Abdelrahman[c] [ID], Hasnat Aslam[d], Abdul Quddoos[a], Rana Waqar Aslam[a], Majid Nazeer[e], Mohammed S. Fnais[c] and Azeem Sardar[f]

[a]State Key Laboratory of Information Engineering in Surveying, Mapping and Remote Sensing, Wuhan University, Wuhan, China; [b]Department of Earth and Environmental Sciences, Bahria University, Islamabad, Pakistan; [c]Department of Geology and Geophysics, College of Science, King Saud University, Riyadh, Saudi Arabia; [d]College of Agriculture and Natural Resources, University of Nebraska-Lincoln, Lincoln, Nebraska, USA; [e]Department of Land Surveying and Geo-Informatics (LSGI), The Hong Kong Polytechnic University, Hong Kong, SAR China; [f]Department of Agricultural Economics, University of Agriculture, Faisalabad, Pakistan

ABSTRACT

Accurate insights into the spatial distribution of cultivated areas, land use for effective agricultural management, and improvement of food security planning, especially in developing countries. Therefore, this study examined the impact of land changes and population growth on agricultural land and wheat crop productivity. First, by incorporating more than three decades of satellite data (1990–2022) and different Landsat missions with machine learning algorithms, high-confidence classes were defined for different land features, including cropland. Second, the wheat grown area was identified using the cropland extraction based wheat acreage assessment method (CLE-WAAM). Third, population dynamics were examined by applying an exponential growth model to forecast population growth and predict food demand. These findings necessitate the integrated methodological development for wheat demand and supply mechanisms using the two-step floating catchment area (2SFCA) approach for a more thorough analysis of socioeconomic developments. The results revealed that the cropland area was transformed into non-cropland, with a percentage of 8.01. A 79% rise in the population occured between 1990 and 2022, with a projected increase of 112% by 2030. Specifically, the wheat cultivation area decreased by 28%, despite stagnant parameters observed since 2000. The proposed method contributes efficiently to the United Nations' sustainable development goal (02: Zero Hunger) using satellite, geospatial, and statistical data integration.

1. Introduction

The global population is estimated to reach nearly 10 billion by 2050, leading to a surge in agricultural demand. Under a scenario of moderate economic growth, this demand is anticipated to increase by approximately 50% compared with the levels observed in 2013. The rise in income in low- and middle-income countries, especially under developing countries, is expected to expedite a shift in dietary patterns, with a greater emphasis on food consumption. This transition necessitates corresponding adjustments in agricultural productivity, including additional stress on natural resources (FAO, 2017).

Current global trends, including rapid population growth, urbanization, abandonment of agricultural land, and climate change, impact food production and security, which also fall into sustainable development goals (United Nation, 2017). The SDG's goal 02 (zero hunger), related to managing and sustaining food supply in the coming decades, will necessitate the efficient utilization of agricultural land and sustainable solutions to meet food demand (United Nation, 2023). However, natural and environmental factors that vary in both time and space play a critical role in determining and influencing agricultural land use (Devkota et al., 2024; Mjiri et al., 2022; Z. Zhang et al., 2024; Q. Zhang et al., 2023). To address

this issue, this study attempts to better identify and assess the factors influencing agricultural land use, land use, and land cover (LULC), including food demand, supply, and socio-economic developments, with innovative integrated approaches across diverse cross-scale and geographical contexts to achieve SDG's goal 02. The rising worldwide need for food, along with rapid urbanization and the extensive effects of climate change (Mjiri et al., 2020; Rahimi et al., 2021; Zeng et al., 2023), highlights the crucial significance of monitoring and analyzing variations in cropland dynamics throughout the years (Aloo et al., 2019; Bouasria et al., 2021a; Bounif et al., 2021; Zambrano et al., 2018). Accurately identifying cropland to other types of land cover is essential for efficient land management and policy formulation of policies (El Mjiri et al., 2021; Shirzad et al., 2022; Wu et al., 2022).

The rising consequences of climate change, combined with uncontrolled expansion and unsustainable agricultural methods, have heightened the worldwide problem of cropland degradation and urbanization, which depends on agricultural productivity worldwide (Mjiri et al., 2022; Pandey & Seto, 2015; Popescu & Popescu, 2022). The transformation of fertile land into other land uses has significant consequences that disturb ecosystems, biodiversity, food security, and the well-being of vulnerable populations (Hou et al., 2021; Rahimi et al., 2022). Conversely, human actions such as deforestation, excessive grazing, inadequate farming techniques, urbanization, and population growth are just a few of the problems endangering land sustainability (Liu et al., 2005; C. Chen et al., 2023). Urbanization and population growth have resulted in the enlargement of cities, leading to the encroachment of agricultural land. Unplanned population growth, rapid urbanization, and the expansion or contraction of agricultural operations are the main drivers of changes in land use and land cover at different spatial scales (Tu et al., 2021). On a daily basis, a substantial number of populations increase and shift LULC patterns, especially in croplands, resulting in considerable pressure on socioeconomic and environmental resources globally (Hailu et al., 2020; Hassan et al., 2016). Therefore, it is necessary to observe drastic effects using advanced methodologies in an appropriate manner (Aslam et al., 2024; Diem et al., 2024). Therefore, the classification of a vast quantity of satellite images and their properties present substantial computing issues related to big data (Bouasria et al., 2021b; Bouslihim et al., 2024). LULC classifiers can be utilized to understand the complexities linked to

floods, droughts, urbanization, agriculture, and other variables at the national, continental, and global levels (Derdouri et al., 2021; Govender et al., 2022; Kavhu et al., 2022). As a result, they can offer LULC products with a better resolution than those currently available. For example, several global land-cover products, such as GlobCover, often possess a lower spatial resolution of approximately 300 m (Jie Wang et al., 2015). The most effective method for acquiring LULC data involves classifying remotely sensed images utilizing several criteria such as spectral signatures, indices, and contextual information for image classification (Alshari & Gawali, 2021; Ehsan et al., 2024). Image classification involves assigning pixels to certain classes based on various criteria such as spectral signatures, indices, contextual information, and other factors (Shi et al., 2019; Vivekananda et al., 2021). It is difficult to implement and analyze the interaction between many parameters and machine learning classifiers on higher-resolution and multitemporal images at a regional scale (Cheng et al., 2023; Sharma et al., 2017).

In many studies, remote sensing (RS) and geographical information system (GIS) utilization practices for cropland have provided generalized estimation equations to evaluate machine learning classifiers, such as classification and regression trees (CART) (Jin Wang et al. 2018), random forests (RF) (Ghosh et al., 2014), support vector machines (SVM) (Jozdani et al., 2019), maximum likelihood classifiers (MLC) (Erbek et al., 2004), artificial neural networks (ANN) (Sajan et al., 2022) and convolutional neural networks (CNN) (C. Zhang et al., 2019). Crop monitoring and management have seen a growing use of earth observation data from sensors such as Sentinel-1C-band Synthetic Aperture Radar (S1 SAR) (Hütt et al., 2016), Sentinel-2 Multispectral Instrument (S2 MSI) (L. Sun et al., 2021), Radarsat-2 (Skakun et al., 2016), Landsat (Graesser & Ramankutty, 2017), and moderate-resolution imaging spectroradiometer (MODIS) (Pittman et al., 2010). Some researchers have also employed satellite images from planet satellites and aerial images for classification (Tao et al., 2020; Vogels et al., 2017). These satellites provide moderate to high geographic resolutions and have been widely used in various research studies. In addition, the need for improved methodology determines that the alteration of LULC is intricate (Valle et al., 2023) which is linked to human activities and can exert a discernible impact on the climate. Population growth, urban development, changes in the local and regional environment, agricultural land depletion, and consumption of natural resources are key factors driving

urbanization (Zahoor et al., 2022) which have been examined with RS and machine learning techniques using efficient processing platforms (Ball et al., 2017; Raza et al., 2024; Sagan et al., 2020). Recently, the manner in which remotely sensed imagery is obtained and examined has changed. Whereas the satellite imagery with the machine learning approach has been able to identify the agricultural land area over a big study area. Instead of utilizing local computers, this procedure is currently being conducted on cloud computing platforms, where data are stored and interactions occur over the Internet (C. Chen et al., 2023; C. Yang et al., 2017). The Google Earth Engine (GEE) is a prevailing and widely used platform in this domain (X. Zhang et al., 2020). This platform provides effortless access to multiple publicly available imagery archives, including Landsat and Sentinel, as well as conventional image-processing tools contained within a high-performance computing environment (DeVries et al., 2020). Cloud-based solutions, such as platforms like GEE, offer parallel processing environments for activities associated with image categorization using satellite image libraries (Amani et al., 2020; Mananze et al., 2020).

Previous studies using remote sensing, machine learning, and socio-economic analysis in this interdisciplinary approach have provided valuable insights for land management, population studies, and food security research separately (Junye Wang et al. 2022; Loibl et al., 2022; Odhiambo et al., 2021). All these factors have a great influence on each other for spatial representation and assessment, with great potential for work enhancement in an integrated framework. The interplay between LULC, specifically regarding agricultural patterns, has a significant influence on worldwide environmental and socioeconomic landscapes (Ahmad et al., 2022; Su et al., 2014). Comprehending the sequential development of agriculture land and its correlation with socioeconomic progress is crucial for sustainable development. Examining temporal agricultural patterns is crucial for decision-makers, environmental scientists, and planners involved in sustainable land management and agricultural planning by incorporating demographic, socioeconomic (Würtenberger et al., 2006) and remote sensing for analyzing human exposure. In the previous literature, most research, especially for developing countries, employs techniques for LULC, population changes, cropland area, and demographic observations separately of the integration of some parameters (Najmuddin et al., 2018; Patel et al., 2019) but however, food consumption and production need

more consideration to overcome food security issues. In 2017, the global food security index (GFSI) was developed for the risk assessment of food security, which has been used previously for country ranking (Odhiambo et al., 2021). The two-step floating catchment area (2SFCA) model has been developed for accessibility mapping and has also been used in food supply to recognize low food access units (X. Chen, 2019). The 2SFCA model has also been used at the community and state levels using catchment information and distant decay functions for accessibility mapping (X. Chen & Jia, 2019). The 2SFCA model is primarily used for accessibility mapping in education, health, and food supply assessments. This research has intensively focused on the integration of remote sensing, demographic, statistical, and socio-economic indicators to provide a comprehensive and technically justified road map for socio-economic development and sustainability in terms of food security and scarcity (Mikalauskiene et al., 2018) but however, gaps exist in previous work. A comprehensive analysis of several aspects associated with wheat (Zhu et al., 2023), such as the extent of cropland, requirement, overall production, and availability per capita, revealed trade-offs (Bakker et al., 2021) between population growth and the need to guarantee sufficient food supply (Z. Xu et al., 2013; Odey et al., 2023).

This study aims to fill the research gaps by using the proposed integrated methodology using remote sensing, population, cropland productivity, and socio-economic factor data. This study is divided into three main sections. First, the cropland extraction (CLE) methodology has been used to examine temporal changes from 1990 to 2022 with scenarios of transitions to non-croplands. Second, the precise CLE mask has been used in the wheat acreage assessment method (WAAM) for identification of precise wheat grown area. Third, the study proposed a comprehensive methodology to analyze wheat demand and supply in an efficient way with population dynamics variables, using the concept of 2SFCA and geographical data integration. This study emphasizes the challenges of maintaining an adequate per capita wheat supply in light of a growing population, showing notable threats to food security. Therefore, research's effectiveness and contributions towards the United Nations' sustainable development goal will help overcome food security with the incorporation of remote sensing, geospatial, and statistical data and provide great insight for sustainability measures.

2. Materials and methods

The selection of machine-learning algorithms is crucial for achieving precise LULC classification. This study evaluated the performance of RF, SVM, and CART in terms of their capacity to distinguish agricultural land patterns over a period of time. In addition, satellite-based indices were calculated and compared to provide a thorough assessment of vegetation vitality and land surface temperature (LST). This study seeks to enhance our comprehensive understanding of the complex interconnections between land use, environmental variables, population growth, and socio-economic advancements by incorporating machine learning algorithms, satellite-derived indices, and socio-economic data. The study proposed a comprehensive methodological framework for cropland, including wheat demand and supply, in an innovative way with diverse data integration using the concept of 2SFCA modeling and geographical data incorporation. The research also includes supervised phenological profiling to explore temporal wheat cultivation patterns that have direct impacts on local communities, livelihoods, the broader economy, and food security. The detailed workflow chart shows the hierarchy of the processing methodology (Figure 1).
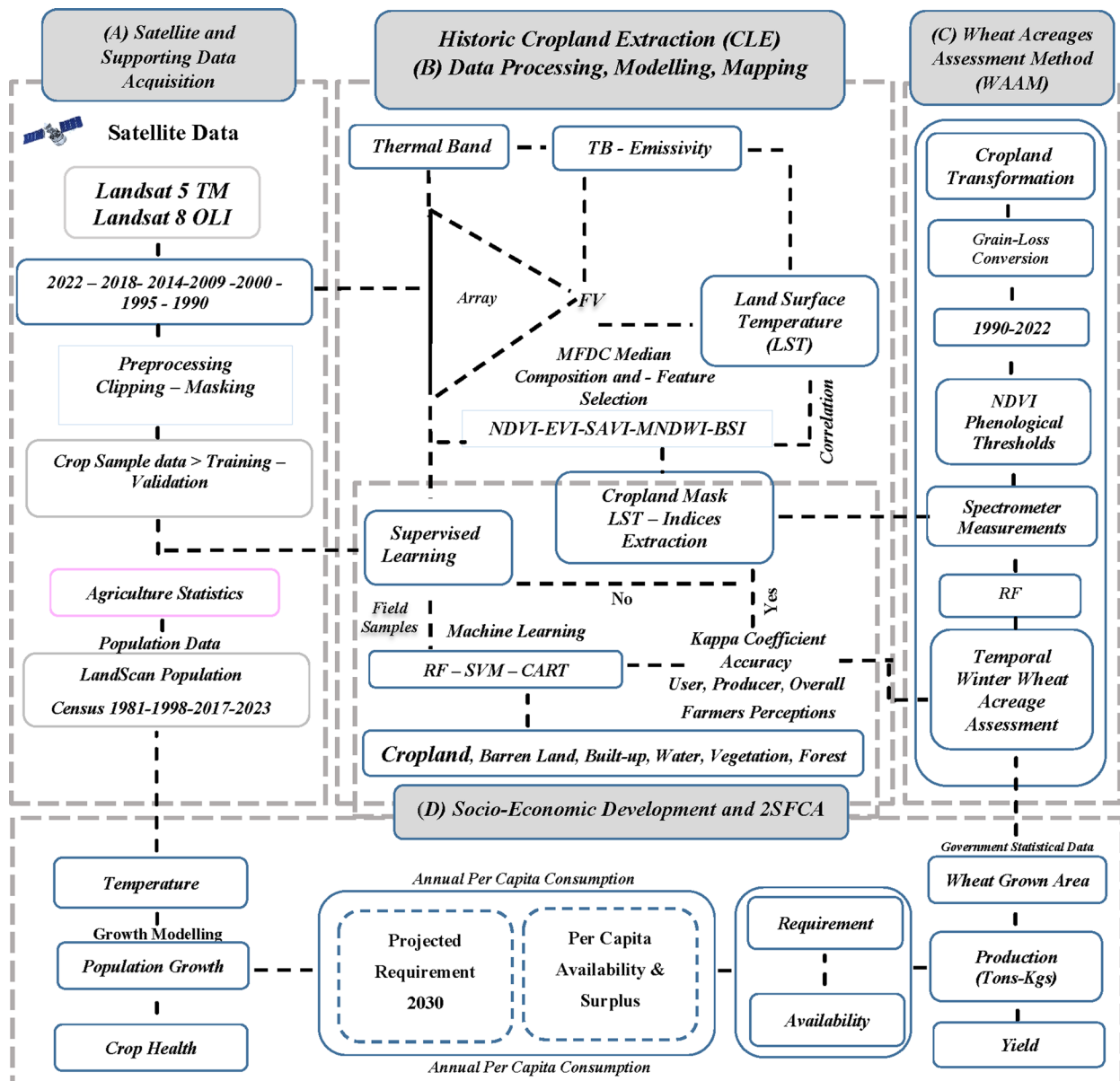

Figure 1. Comprehensive workflow diagram.

2.1. Study area

The current research investigation was carried out in the Sahiwal district, located in the central region of Punjab Province, Pakistan, which is renowned for its varied agricultural terrain. The study region extends from 30.6682° N to 30.7682° N latitude and 73.1114° E to 73.2114° E longitude, spanning approximately 3,200 square kilometers (Figure 2). The Sahiwal district is situated in the productive plains of the Chenab and Sutlej Rivers, known for its varied landscape and prosperous agricultural history (Hussain et al., 2023). The region displays diverse agricultural patterns, including crops such as wheat, maize, rice, sugarcane, cotton, and several horticultural crops (Irfan et al., 2022). Wheat is the primary crop, indicating the agricultural importance of this region (Raza et al., 2024). Sahiwal has exhibited significant demographic shifts based on data from the 1981, 1998, 2017, and 2023 censuses. The populations reported for these years were 1,281,526, 1,843,194, 2,513,011, and 2,881,811, respectively. The demographic changes observed in this region reflect its dynamic character and have the potential to significantly influence land utilization and socioeconomic issues in the long run.

2.2. Dataset and preprocessing

The datasets used in this study consisted of spectral bands, specifically blue, green, red, NIR, and SWIR, obtained from Landsat 5 thematic mapper (TM) and Landsat 8 operational land imager (OLI) sensors. Which has been preprocessed included image enhancement and masking, where the acquisition of satellite images was based on the cloud conditions, which were set to standard < 5%, which varied with climate conditions. Vegetation, non-vegetation indices, and land surface temperature (LST) were calculated using the same Landsat images for temporal periods (Hussain et al., 2023). Population density data from 2000 to 2022 were acquired from the LandScan Global and official census data sources. In
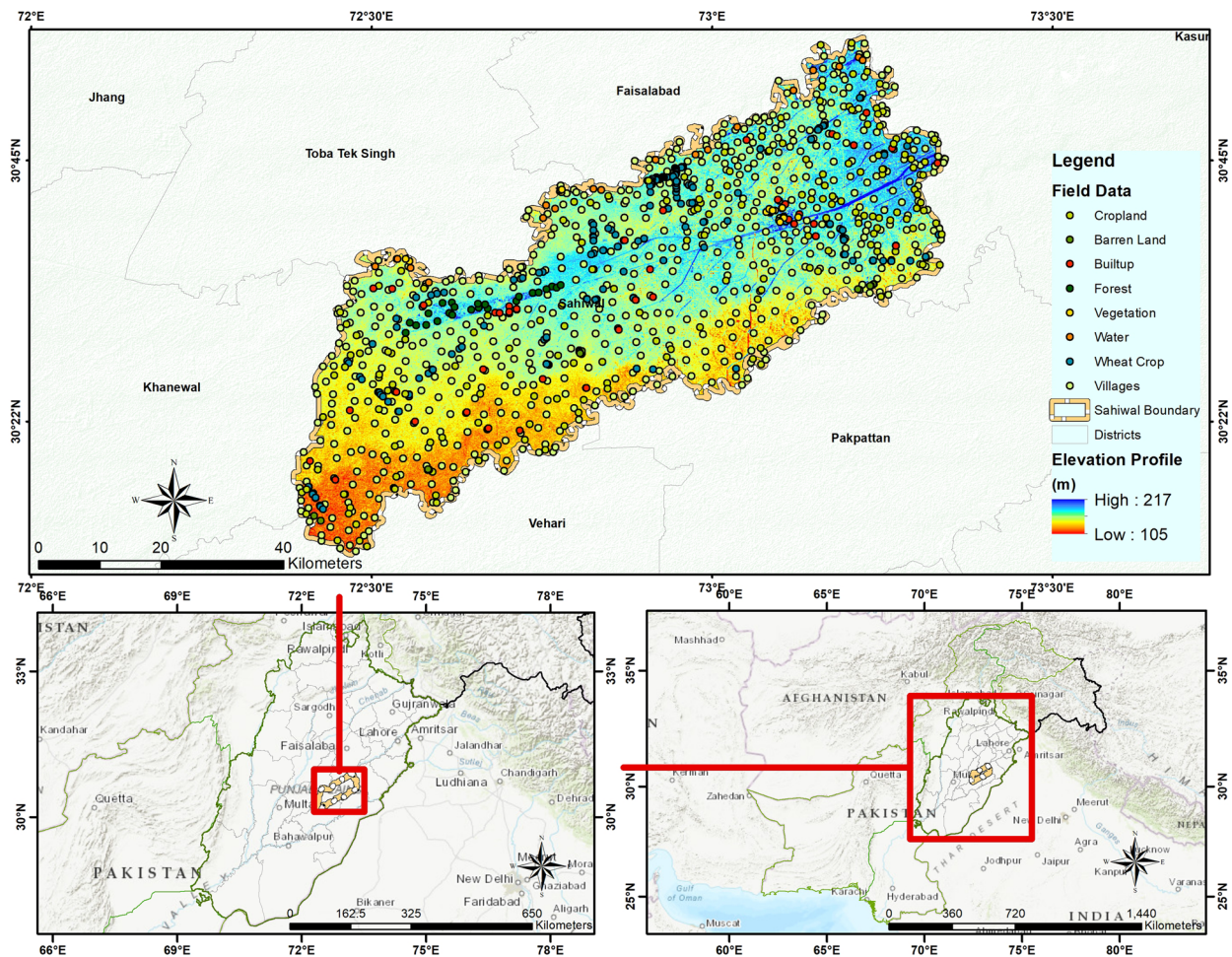

Figure 2. Geographical representation of study area by sample data and settlement information with elevation profile from SRTM-DEM with 30-meters spatial resolution.

Table 1. Dataset used for the study by their characteristics with sensor and related information.

Datasets	Characteristics	Sensor	Temporal extent	Source
Blue	Spectral bands	Landsat 5TM & Landsat 8 OLI	1990	USGS
Green		30 meters Resolution	1995	United States Geological
Red			2000	Survey
NIR			2009	
SWIR			2014	
NDVI	Spectral vegetation and		2018	Derived from Landsat 5 and
EVI	non-vegetation indices		2022	Landsat 8
SAVI				
MNDWI				
BSI				
LST	Surface temperature			
Population	Population density	LandScan Global & Census	2000 – 2022	https://landscan.ornl.gov/ https://www.pbs.gov.pk/ https://www.citypopulation.de/
Sample Data	Signatures	Field Observations-Google Earth & Phenological Profiling	Field Visit 2022 - Temporal Signature VHR - Google Earth	–
Statistical Data	Crop statistics	–	–	CRS

addition, the sample data included signature information derived from field observations (1861 cropland samples) and very high-resolution (VHR) Google Earth (GE) images from the GE platform, continuing temporal features. The statistical dataset contains crop-related data, which serve as a complete basis for studying the temporal patterns of farmland and their socio-economic consequences in the Sahiwal area of Pakistan. The multiple datasets used in this study were obtained from the United States Geological Survey (USGS), Oak Ridge Laboratory (ORL), Agricultural Department, and National Census Data Center (Table 1). These databases provide a comprehensive analysis that combines remote sensing, demographic information, and ground-truth data.

2.2.1. Spectral vegetation and non-vegetation indices

In this study, a wide range of vegetation and non-vegetation indices were specifically tailored to extract different information from Landsat 5 and 8 images (S. Pal & Ziaul, 2017). Blue, green, red, NIR, and SWIR bands were used in the indicated indices for Landsat 5 and 8 with sequence as 1–5 and 2–6, respectively, for both outcomes (Table 2). However, due to canopy cover, NIR shows high reflectance for healthy vegetation and is less absorbed by water. For vegetation and soil moisture, the SWIR was sensitive to moisture content. The collection of indices in this array allowed for a detailed examination of temporal cropland patterns, vegetation health, and overall changes in land cover in the Sahiwal region.

The NDVI measures the health of vegetation, with higher values indicating healthier vegetation and lower values potentially indicating non-vegetated surfaces or stressed vegetation. The EVI is used to reduce the impact of atmospheric factors and to consider differences in the arrangement of vegetation, resulting in more precise evaluations of vegetation conditions. The equation (Table 2) includes the following components: L, which represents the canopy background adjustment with a value of 1.0; C1 and C2, which are the coefficients of the aerosol resistance term with values of 6.0 and 7.5, respectively; and G, a scaling factor with a value of 2.5. SAVI is particularly successful in regions with limited vegetation or high soil brightness because it reduces the impact of soil reflectance. In this study, a soil-adjusted factor (L) of 0.5 was utilized, with higher values indicating healthier vegetation. The MNDWI is particularly effective in identifying variations in surface water over a period of time. Water had higher positive values, while soil and vegetation continued to have negative values in the observations. This is because soil reflects more SWIR light than near-infrared light, whereas vegetation reflects even more SWIR light than green light. BSI can differentiate between exposed soil and vegetation, rendering it highly useful for monitoring agricultural regions. Elevated values indicate the presence of bare soil, whereas lower values indicate the existence of vegetated areas.

2.2.2. Land surface temperature retrieval

LST was calculated using corrected thermal infrared images from Landsat Thematic Mapper (TM) for 1990, 1995, 2000, and 2009, and from Landsat 8 OLI for 2014, 2018, and 2022. The calculation of LST involves the use of thermal infrared bands derived from remote sensing data (Sohail et al., 2023). The Stefan-Boltzmann Law (Equation 1) are frequently employed in mathematical expressions

Table 2. Indices driving equation used for Landsat 5 TM and Landsat 8 OLI.

Sr	Index	Satellite	Equation	Reference
1	NDVI	Landsat 05 Thematic Mapper	NIR- Red/ NIR+ Red	(Rouse et al., 1973)
2	EVI	Landsat 08 Operation Land Imager	G × ((NIR - Red) / (NIR+C$_1$ × Red − C$_2$ × Blue+L))	(Moura et al., 2012)
3	SAVI		(NIR - Blue) / (NIR+Blue+L) × (1×L)	(Huete, 1988)
4	MNDWI		Green- SWIR/ Green+SWIR	(H. Xu, 2006)
5	BSI		(Blue+SWIR) - (NIR+ Red) / (Blue+SWIR) + (NIR+Red)	(Piyoosh & Ghosh, 2018)

*NDVI: normalized difference vegetation index; EVI: enhanced vegetation index; SAVI: soil-adjusted vegetation index; MNDWI: modified normalized difference water index; BSI: bare soil index; NIR: near-infrared; SWIR: shorter-wave infrared.

(Kafy et al., 2021; Qadri et al., 2023; Ullah et al., 2019). Consequently, adjustments for emissivity (ε) are required based on the characteristics of land cover (Equation 2). To consider the impact of vegetation on thermal infrared values, this study also employed the fractional vegetation (FV) index. The FV (Equation 3) The index is computed using a mathematical calculation, and the computation of FV relies on the NDVI measurements in order to improve the precision of estimating LST.

The LST for the retrieval of surface temperature, including the fractional vegetation (FV), was evaluated using the following equations:

$$LST = \left(TB \Big/ \left(1 + \left(\lambda \times \frac{TB}{\rho} \times \ln(\epsilon) \right) \right) \right) - 273.15 \quad (1)$$

$$\epsilon = a \times FV + b \quad (2)$$

$$FV = \left(NDVI - NDVI_{min} \Big/ NDVI_{max} - NDVI_{min} \right)^2 \quad (3)$$

where *TB* brightness temperature of sensor, λ emitted radiance wavelength, constant value obtained from Boltzman and ε is emissivity. In the upper equation FV is the fractional vegetation index, a and b are constants, the $NDVI_{min}$ is the lowest NDVI value, and $NDVI_{max}$ is the highest NDVI value.

When NDVI readings were below 0.2, the surface was predominantly covered with bare soil. In this case, an emissivity value of 0.97 is applied. The NDVI values ranging from 0.2 to 0.5 indicate a combination of soil and vegetation cover (J. A. Sobrino et al., 2004; Orhan & Yakar, 2016; Jose A. Sobrino et al., 2008). To determine the emissivity value for such mixtures, the following equations are utilized: NDVI values exceeding 0.5, indicating full vegetation coverage on the surface, and an emissivity value of 0.99 is assigned in such cases.

$$\epsilon = 0.004 \times FVC + 0.986 \quad (4)$$

These calculations were used to approximate the surface temperature and emissivity (Equation 4) Using thermal infrared data collected from satellites or aerial sources. They play a crucial role in applications, such as environmental monitoring, agriculture, and urban heat island studies.

2.3. Training and feature data selection for cropland extraction (CLE) with LULC classes

The study combined Landsat spectral bands (blue, green, red, NIR, and SWIR) with five key spectral indices and LST data using the mega file data cube (MFDC) for the Rabi (winter-spring) and Kharif (summer-autumn) seasons, which used the MFDC process of prior research (Raza et al., 2024). These datasets spatial resolution has been set at 30 m and cover the period 1990–2022 for both seasons; each observed year starts from November for MFDC. These datasets were integrated together using an MFDC; this method is particularly effective in remote sensing (Gumma et al., 2020; Raza et al., 2024), as it is useful for the analysis of diverse datasets and improves the precision of classification. The combined spectral and thermal bands helped the classifiers distinguish differences between cropland, other vegetation, and built-up areas. This integration improved both the accuracy and reliability of the classifications. Seasonal temperature variations of LST can align with crop phenology (i.e. sowing, flowering, harvesting stages). The thermal data also has the ability to detect surface temperature variations complemented by the spectral indices. Meteorological variables, such as temperature, have a very smooth gradient as compared to other variables, and it is not abruptly changed in nature until there is a huge variation in terms of elevation and land uses. The classification requires distinguishing between spectrally similar classes with different thermal behaviors (i.e. cropland vs. barren soil). The LULC classification algorithms used in this study were based on a sample dataset gathered in 2022 supplemented by temporal LULC dynamics, which were also derived from VHRGE. A field survey was also conducted in 2022 for LULC assessment in the study area for precise feature identification using remote sensing sensors (Zhang et al., 2019) as a training dataset (Figure 3). The dataset is
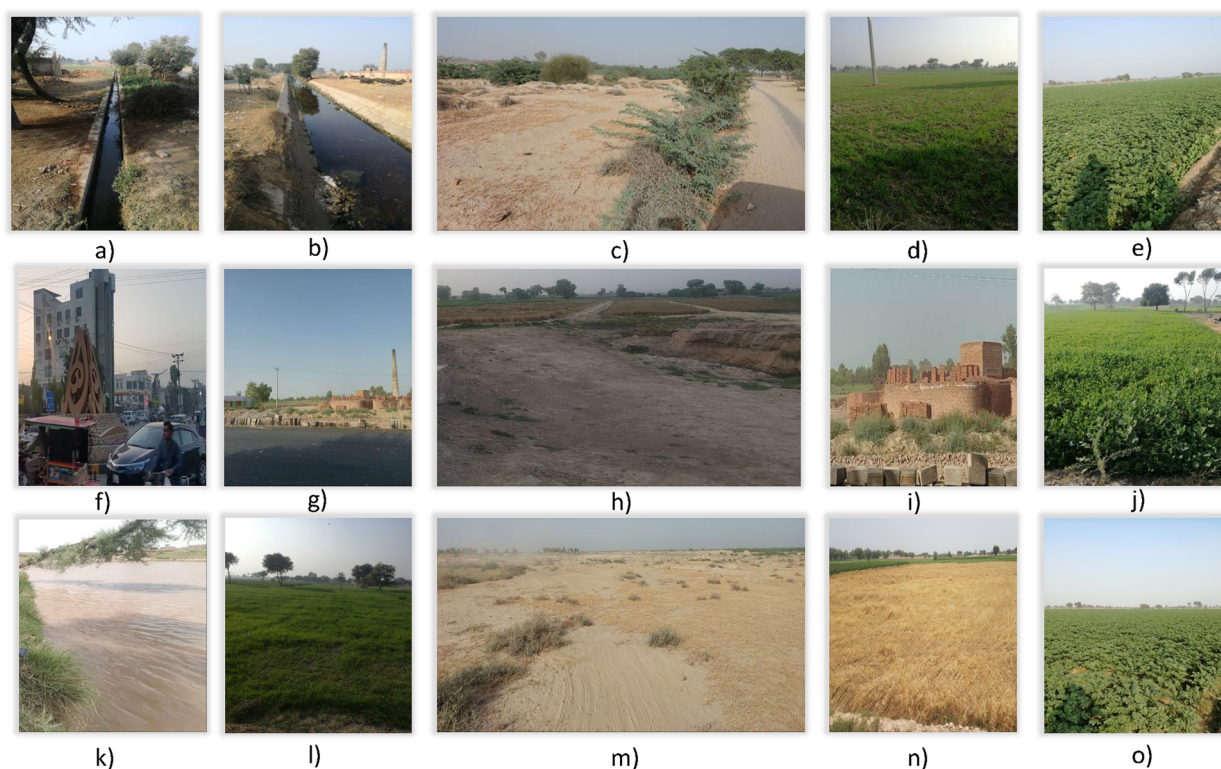
Figure 3. Field sample data location in the observed area with photos taken during the survey in 2022.

highly comprehensive and offers intricate data on subclasses within the study region, which forms a strong basis for subsequent supervised classification techniques.

The sample data necessary for these methods were obtained from Landsat satellite images, notably Landsat 5TM and Landsat 8 OLI, which cover the period 1990–2022. Meticulous selection and organization of the training dataset are crucial for achieving precise and widely applicable model results. In this research, feature selection data were gathered during the field survey and from Google Earth high-resolution imagery. Feature sample data selection for temporal images has taken place through the integration of multiple spectral images, the comparison of RGB false color composites of multi-temporal and multi-sensor Landsat scenes, and GE high-resolution imagery. Thus, the feature selection process was based on the spectral and temporal features of the study area, with some constraints. In addition to the NDVI (- to +1), the maximum values indicate forest cover areas and healthy vegetation, including cropland, and the lowest values indicate artificial surface and water bodies. Soil-adjusted vegetation index (SAVI) has been used to reduce the influence of soil on vegetation in mixed-pixel areas (da Silva et al. 2020). The enhanced vegetation index (EVI) was used for canopy

Table 3. Classified classes hierarchy with subclasses and id information used in the classification.

Code	Classes	Subclasses
0	Agriculture	Cultivated Land, Crop Land
1	Built up	Settlement, Urban, Rural
2	Barren Land	Uncultivated, Bare Soil, Barren
3	Vegetation	Shrubs, Grass, Sparse Vegetation, Orchards
4	Water	River, Canal, Ponds, Fish Farm
5	Forest	Forest cover, Included Trees Species

greenness in an area (Jafari et al., 2017), which was further used to discriminate among several vegetation types. The bare soil index (BSI) (Liu et al., 2022) and modified normalized difference water index (MNDWI) (Hossain et al., 2024) spectral responses show distinctions between bare soil and water bodies and highlight the areas with fluctuations in their spectral responses, respectively. Every sample in the training dataset was linked to distinct land-cover categories, including cropland, barren land, built-up land, vegetation, forest, and water (Table 3). Careful curation and preprocessing of the training data are crucial for guaranteeing the precision and applicability of the model (R.-C. Chen et al., 2020). This procedure entails instructing the machine learning algorithm on the complex connections between input characteristics, such as spectral bands and indices, and their corresponding land-cover classes. By using the training data for all land use land cover

classes on Landsat satellite utilizing the GEE platform, the model's capacity to discern subtle differences among different land cover categories within the designated research area was observed.

2.4. Machine learning algorithms for cropland extraction (CLE) with LULC classes

Classification, in the context of machine learning, refers to a type of supervised learning in which a given dataset is analyzed and a model is constructed to categorize the data into a predetermined number of classes (Goldblatt et al., 2018). This study provides a thorough evaluation of various machine learning methods (RF, SVM, and CART) used to classify temporal agricultural patterns from 1990 to 2022, utilizing satellite images from Landsat 5 and Landsat 8 with several spectral indices. These algorithms have been selected because of their distinct capabilities and advantages regarding classification, particularly in cropland and LULC extraction, by an insightful understanding of previous methodologies (Adam et al., 2014; Le et al., 2022; Rana & Venkata Suryanarayana, 2020; Tariq et al., 2023; Zhao et al., 2024). To maintain the overall distribution in the study region, a random sampling method was used to ensure the distribution of sample data. Whereas, A split of 0.8 has been used for the classification of satellite data, with 80% of the sample used for training and 20% for the validation of the data. The training sample dataset of six LULC classes, including cropland, was applied to satellite images using three ML algorithms for classification, as described below.

2.4.1. Random forest

The RF algorithm is an ML technique that utilizes a collection of independent decision trees known as RF classifiers. These decision trees were created by randomly selecting subsets of the original dataset and then combining their predictions into categories of new data points. The mode of all decision-tree predictions serves as the basis for the final classification (Z. Sun et al., 2024). As the number of trees increased, the general precision of the classification improved without overfitting. Each tree independently classifies the input and selects the most common class through voting (F. Zhang & Yang, 2020). In addition, RF utilizes a bagging technique in which each tree randomly chooses a subset of features and training data with the possibility of replacement (Breiman, 2001). Additionally, the RF provides

insight into the features of the raster data with the contribution of spectral indices (Aeman et al., 2023) such as NDVI, SAVI, EVI, MNDWI, and BSI with LST layer. The random forest ML algorithm is an ensemble constructed from the components of the multiple trees to make a decision for the resultant layer. Furthermore, (Feng et al., 2015) noticed that the RF with selected 200 decision trees in their study had higher performance. The algorithm is a supervised ML method that operates on defined decision trees to assign classification.

2.4.2. Support vector machine

It is a pivotal classifier in the field of pattern recognition, which is a highly popular and dynamic area of research among scholars (Mountrakis et al., 2011; Zhao et al., 2024). SVM is a very efficient classifier that seeks to create an optimal hyperplane for distinguishing between distinct classes, with the goal of minimizing the number of incorrectly classified cases throughout the training process (Shih et al., 2019). The hyperplane divides the data into separate predetermined classes using kernels based on training data. The SVM employs a kernel to convert nonlinear datasets into a feature space of greater dimensions. Additionally, variables such as the choice of training samples, the size of the sample, and the variety of data all have an impact on the accuracy of these complex systems are (Ayat et al., 2005). Based on the research of M. Pal (2008), it is beneficial to select parameter C using an exponentially expanding sequence to obtain more accurate results. C is a scale parameter that improves the performance of the model by improving the approximation of the optimal values. The SVM also provides high-dimensional suitability for remote sensing data with several spectral bands. To overcome the issue of large-scale data, this study also utilized an efficient training sample distribution with parameter tuning to mitigate the risk. Additionally, hyperparameter tuning with the grid search and cross-validation process ensured the accuracy of the model. This study also achieved an effective and comprehensive approach for temporal cropland and LULC extraction, with accurate and interpretable results. Previously, the highest kappa value was obtained for SVM using a principal component analysis (PCA) based approach (Rana & Venkata Suryanarayana, 2020). In addition, SVM has gained popularity as a classification approach owing to its strong theoretical foundations and ability to enhance classification.

2.4.3. Classification and regression tree

CART methodologies are commonly employed in the remote sensing field to classify, plot, and model data. Regression trees are used to analyze the relationship between a single continuous response variable and multiple explanatory variables, which can be continuous or discrete. This is achieved through a process called binary recursive partitioning, where the data are split into increasingly homogeneous nodes using combinations of rules that best differentiate the variation in the response variable (Y. Wang et al., 2021). The method functions by repetitively partitioning the node until it reaches the terminal nodes according to a pre-established edge (Choubin et al., 2018). Although CART may exhibit a propensity to overfit the model to some extent, its rapid performance and precise results have established it as one of the most frequently employed classifiers for LULC (Zhao et al., 2024). In this study, the cloud platform with input parameters "classifier. smileCART" is used for categorizing LULC with training data and its versatility in handling classification and regression tasks (Feizizadeh et al., 2023).

2.5. Validation and accuracy assessment

The accuracy of the three ML algorithms (RF, SVM, CART) results was observed using the confusion matrix accuracy assessment method using the validation data samples (S. Pal & Ziaul, 2017). The user, producer, and overall accuracy were assessed for all three temporal ML classifier results separately with validation kappa. This process helps evaluate the efficiency of these classifiers in the test case of the observed study area. Later, the accuracy of wheat-grown area was assessed using the same confusion matrix method across all temporal datasets. The identified temporal wheat area was also compared with the available statistical data from the Punjab Agriculture Department, Pakistan.

2.6. Temporal cropland pattern distinctions

The categorized data were employed to derive cropland layers throughout several time periods, encompassing 1990–2022. The temporal analysis aimed to detect variations (Akinyemi et al., 2016; Zewude et al., 2022) in cropland areas throughout several time intervals: 1990–1995, 1995–2000, 2000–2009, 2009–2014, 2014–2018, and 2018–2022, and at two specific points in time: 1990 and 2022. Spatial analysis of land cover transitions (SALCT) and land change

trajectory (LCT) methodologies were used to identify and analyze changes in cropland patterns over the observed period. Moreover, cropland pattern distinctions were observed in two categories: one that determined the cropland gain loss (Zhong et al., 2022) and the other that determined the cropland transformations (Drummond et al., 2012).

2.7. Wheat acreages assessment method using CLE mask

This study focused on socioeconomic growth, particularly in regions where wheat was cultivated. Landsat 5 and 8 satellites were used because of their well-known ability to capture a wide range of land cover changes, moderate spatial resolution, and temporal multispectral capabilities (Wulder et al., 2019). The acquisition of wheat is observed through the NDVI of the wheat crop season, which occurs from November to May. Wheat is sown from November to December, while heading to flowering, ripening, and maturity stages occur during the months of January, February, and March, and April-May as harvesting months. The subsequent procedure entailed computing NDVI using a series of Landsat images taken during the winter wheat growing season (L. Sun et al., 2021), which spans from November to May. By observing the changing patterns of the NDVI profiles over time, it was possible to find unique reflectance patterns that were connected to the growth stages of winter wheat (Zhu et al., 2023) to establish the threshold by the field sample with NDVI profiling. The wheat area was examined and identified using phenological profiling, spectroscopy data, processing and modeling of satellite data (G. Yang et al., 2021), which is based on variations in phenological patterns and spectrometer field measurements. These measurements have also been used to generate the field sample data of previous years.

The sample data were generated using the NDVI profiling curve and spectroscopic measurements for wheat identification by observing the behavior of wheat crop trends and growth from the cultivation to the harvesting stage. In addition, in the observed region, the wheat crop season can easily be compared with other crops because of seasonal variation, which can reduce the redundancy of multiple crops. The phenological observation of wheat crops shows that in the crop season months of January, February, and March, the NDVI behavior is much higher than that of other crops (Duan et al., 2017), as the

measurements from spectrometer based NDVI were 0.92, 0.85, and 0.74 for these months, respectively. Additionally, the winter season reduces the impact of other crops (due to phenological cycle), including vegetation, compared to the summer season crops. The NDVI values of other vegetation, such as forest, grass, and shrub areas, were lower than those of wheat during the peak growth (January-February) stage (C. Zhang et al., 2019). Region-specific NDVI thresholds were established based on field survey samples and ground information (Figure 13) with phenological segmentation. The wheat crop signature behavior in peak month reports was greater than 0.57 in NDVI observations. The figure also identifies the detailed threshold observation for the rest of the months, along with the respective peak and trough of the signature, for all wheat fields that have been observed. Later, these were used in the classified seasonal cube for wheat identification. Additionally, the NDVI profile has been identified with a pure field signatures verified with a spectrometer peak curve and phenological regional crop cycle, which has fluctuation in the chlorophyll throughout the phenological cycle observed to define the threshold as an input parameter for classification with Landsat spectral bands. After threshold identification using the field data, all values are set to zero except the values of the defined threshold for the wheat. The method (WAAM) utilized the Landsat spectral bands, NDVI thresholds layer with SAVI and EVI layers in conjunction with the CLE mask to minimize false positive errors. CLE (cropland extraction) mask was generated using an RF classifier applied to the entire study area. The CLE mask was used to improve classification robustness by eliminating non-agricultural land and its impact on the spectral mixing of pixels to improve the wheat fields identification. Landsat spectral bands, including red, green, blue, NIR, SWIR, NDVI thresholds, SAVI, and EVI layers, are purely used to support the RF classification.

NIR and SWIR are crucial for identifying vegetation health and moisture content, whereas the visible bands are also useful for wheat discrimination in the Rabi season. These images were designed to highlight the unique spectral properties of blooming and actively growing wheat (Cao et al., 2018). The RF classifier was trained using both NDVI profiles and Landsat spectral bands to differentiate wheat from other crops. The purpose of this process was to facilitate the supervised classification of wheat signatures, which were derived from NDVI profiling and spectroscopic measurements. To streamline the

identification process, a supervised machine learning method was utilized, specifically, the Random Forest classifier. The wheat signatures were used for training and validation for 2022, where training data were prepared by NDVI phenological observations (758 samples) and validated using field data gathered in 2022 (425 samples) for classification. Whereas, for the rest of the years, the generated wheat sample was divided by split (0.7), in which 70% of signatures were used for training and 30% for validation. The sample size was set at 623, 616, 651, 525, 483, and 504 for training and 267, 264, 279, 225, 207, and 216 for validation in the persistent time period, that is, 2018, 2014, 2009, 2000, 1995, and 1990, respectively. The wheat area for each observed year is identified in km^2 and acres due to the small farming practices. The accuracy of the categorization was evaluated by comparing it to the ground truth points obtained from field surveys and phenological observations. The accuracy assessment using the confusion metric accuracy method was computed by utilizing an independent validation dataset obtained from field data. This method was applied using the crop-masked layer prepared earlier to reduce the effect of other land-use classes for accuracy enhancement. The integration of phenological profiling, NDVI calibration with SAVI, EVI, and CLE masking ensures its reliability and practical applicability for agricultural monitoring. The method demonstrates the ability to enable precise wheat classification across diverse agro-ecological zones and according to their respective time periods.

2.8. Socio economic distinctions

2.8.1. Predictive population growth
The growth pattern in the study area was observed using LandScan population density data for further evaluation (Raza et al., 2024) and forecasting of the population growth analysis utilized by the exponential growth model (EGM), which is represented in Equation 5 (Hobbie & Roth, 2007; Olanrewaju et al., 2020). The basis for extrapolating population estimates for the past and current year census data for 1981, 1998, 2017, and 2023. This model was used to forecast population growth by projecting the population from 2023 to 2030. The model (Equation 5) shows the predicted results for population growth, that is, X_t is the population at time t.

$$X_t = X_0(1+r)^t \qquad (5)$$

where X_o is the initial population at the observed time and r and t represent the growth rate and time, respectively, as shown in the equation above.

2.8.2. Socio economic developments and wheat demand—supply

A thorough assessment of socio-economic progress and possible risks to food security requires a detailed examination of the patterns of wheat cultivation selected by considering threats. The wheat crop areas for 1990, 1995, 2000, 2009, 2014, 2018, and 2022 were determined using satellite images and available agricultural departmental data. The evaluation examined the health of seasonal wheat crops during their growth period using surface temperature data to assess the thermal conditions during important growth stages as a primary indication. The analysis also employed agricultural statistics by including socio-economic elements, such as the yearly per capita wheat consumption, which was set at 124 kg per capita (USDA, 2015). A socioeconomic analysis was conducted to assess the population, wheat requirement, and production (kg/t), and the per capita availability of each year was estimated (Table 4). The purpose was to identify any surplus or prospective deficiencies in the wheat supply. This study utilized a dynamic forecasting method to predict the annual per capita wheat consumption in the study area to determine the overall wheat demand in 2030 (t) by employing the methodology (Mottaleb et al., 2022) using Equation 6 aggregated wheat demand (AWD).

$$AWD_t = PC_t \times PP_t \qquad (6)$$

where t represents the time or year, PC_t is measured for per capita wheat consumption in kilograms, and PP_t represents the population in a year.

The comprehensive approach employed in this study allowed for a detailed understanding of the wheat farming environment and facilitated the detection of possible risks to food security. The concept of the two-step floating catchment area (2SFCA) model (Kuo, 2021; Tao et al., 2020), In this research, spatial demand and supply relationships were identified with defined catchment boundaries (X. Chen & Jia, 2019; Bell et al., 2013), which shows the location-based demand and supply distribution with wheat crop accessibility in the union council (UCs) level catchments that have been threatened by land use and reduction of wheat cultivation. This was the first study to analyze wheat demand and supply using population dynamics, demand, and supply variables for the

Table 4. Socio-economic indicators by remote sensing and statistical data from the years 1990 to 2022.

Sr. no	Data	Source
1	Population	EGM
2	Crop Health	NDVI
3	Temperature	LST
4	Wheat Grown Area	Remote Sensing/ Crop
5	Annual Per Capita Consumption (kg/person)	Reporting Service
6	Production	

year 2022. In the first step, the LandScan gridded 1*1 km dataset was generated within each defined union council (UC) level catchment and corporate with the classified built-up data as demand locations and supplies from the wheat grown area of a 1 km square box to reduce the redundancy and catching smoothness of data. In the first step (Equation 7), the supply to-demand ratio R_j is determined by dividing the capacity of a facility S_j (wheat area–supply) by the total population P_k (population–demand) located within a specified distance d_0 (UC boundary area–calculated by each 1×1 grid within UCs). The second step involves calculating accessibility index A_i for the demand point by summing the R_j values obtained in the first step, as shown in Equation (8).

$$R_j = \frac{S_j}{\sum_{k \in} \left\{ d_{kj} \leq d_0 \right\}^{P_k}} \qquad (7)$$

$$A_i = \sum_{j \in \{d_{ij} \leq d_0\}} R_j = \sum_{j \in \{d_{ij} \leq d_0\}} \frac{S_j}{\sum_{k \in} \left\{ d_{kj} \leq d_0 \right\}^{P_k}} \qquad (8)$$

The aggregated demand that comes from different locations is identified and aggregated supply (wheat production; calculated by yield average 34.5 Â maund per acre, where 1 maund = 40 kg defined by the agriculture department and classified wheat grown area in each UC) coming from different locations. In the second step, the accessibility ratio of each UC is calculated using aggregated demand and supply data. Utilizing satellite data, analyzing consumption trends, and considering population dynamics are essential methods for predicting and tackling past, present, and future issues related to food security. The data sources used for the socioeconomic development assessment are shown in Table 4.

3. Results

3.1. Comparative CLE layers and accuracy assessment

The land cover classification results for Sahiwal were obtained using three machine-learning algorithms:

RF, SVM, and CART. The classification outcomes are displayed in square kilometers for each land cover category for the years 1990, 1995, 2002, 2008, 2013, 2018, and 2022 (Figure 4). The algorithms were used to classify the study region into six main categories: cropland (CL), barren land (BL), built-up (BU),

vegetation (VE), water (WT) and forest (FR) (Figure 5). As seen in the accuracy assessment (Figure 6), the classification results showed better accuracy in the temporal classification scenario with RF, the observed highest accuracy of 95.22%, with kappa of 0.94, compared to the SVM and CART. The cropland area
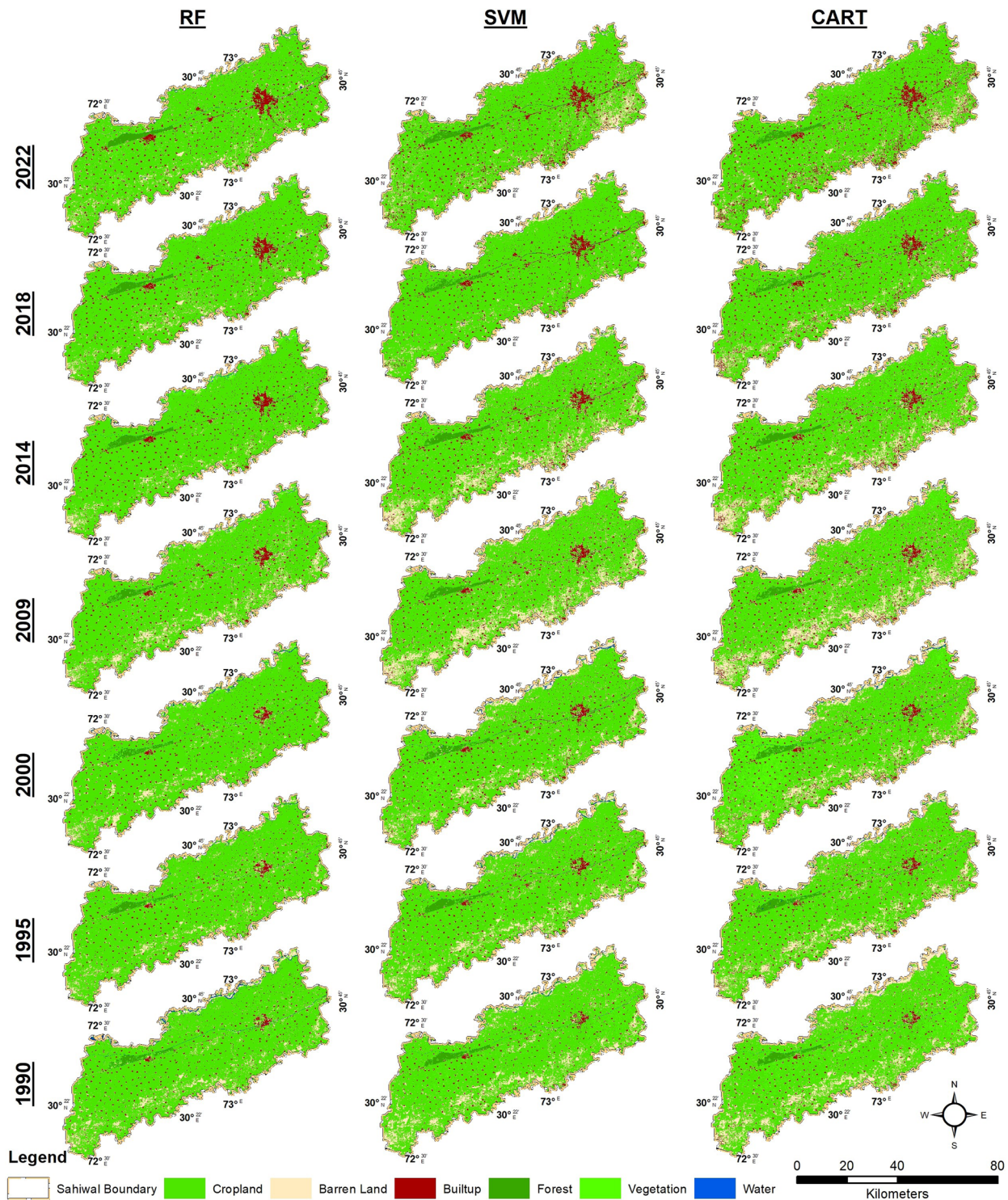

Figure 4. Comparative outcomes of three ML Algorithms i.e. RF-SVM-CART using temporal Landsat 5TM and Landsat 8 OLI satellite images.
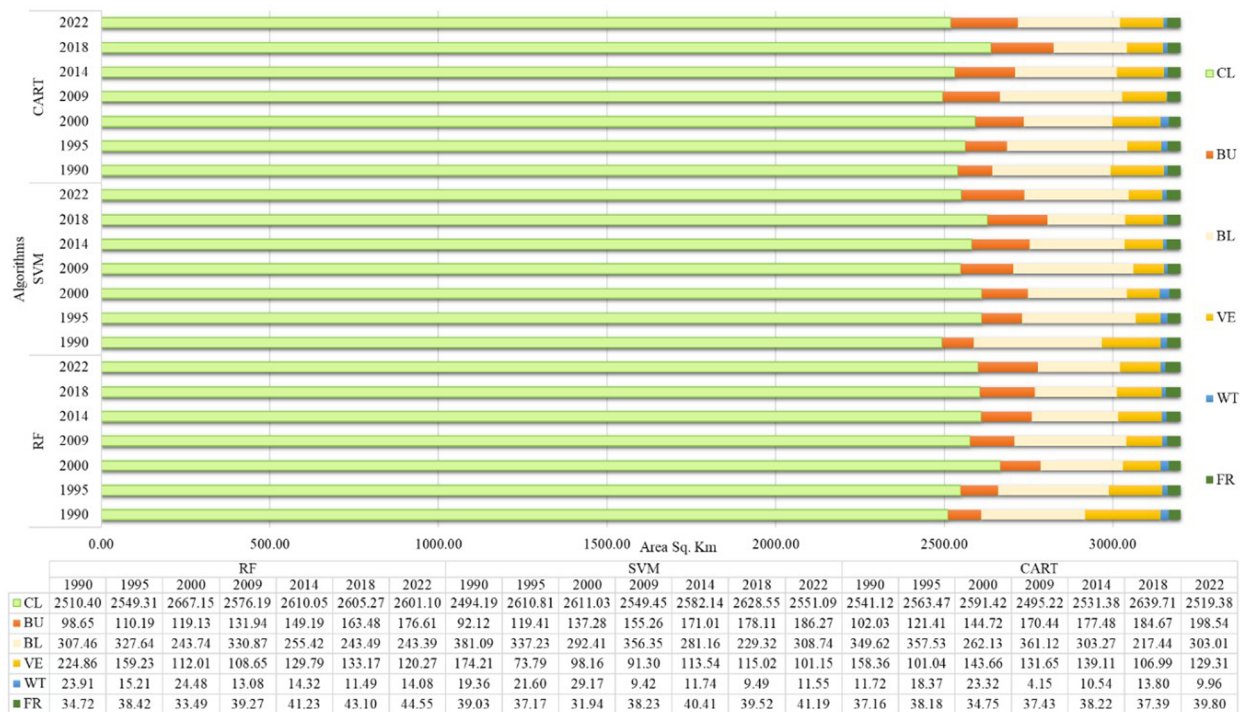
Figure 5. Comparative temporal area by RF, SVM, CART ML algorithms in square km from 1990 to 2022.

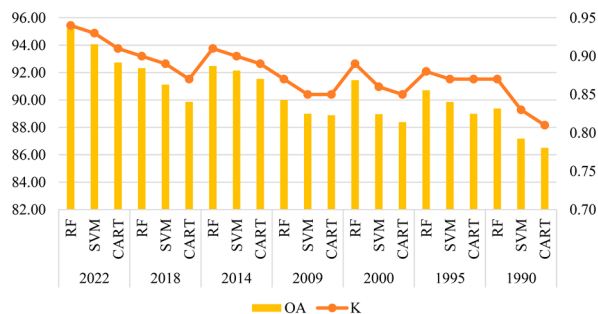|	RF							SVM							CART						
	1990	1995	2000	2009	2014	2018	2022	1990	1995	2000	2009	2014	2018	2022	1990	1995	2000	2009	2014	2018	2022
CL	2510.40	2549.31	2667.15	2576.19	2610.05	2605.27	2601.10	2494.19	2610.81	2611.03	2549.45	2582.14	2628.55	2551.09	2541.12	2563.47	2591.42	2495.22	2531.38	2639.71	2519.38
BU	98.65	110.19	119.13	131.94	149.19	163.48	176.61	92.12	119.41	137.28	155.26	171.01	178.11	186.27	102.03	121.41	144.72	170.44	177.48	184.67	198.54
BL	307.46	327.64	243.74	330.87	255.42	243.49	243.39	381.09	337.23	292.41	356.35	281.16	229.32	308.74	349.62	357.53	262.13	361.12	303.27	217.44	303.01
VE	224.86	159.23	112.01	108.65	129.79	133.17	120.27	174.21	73.79	98.16	91.30	113.54	115.02	101.15	158.36	101.04	143.66	131.65	139.11	106.99	129.31
WT	23.91	15.21	24.48	13.08	14.32	11.49	14.08	19.36	21.60	29.17	9.42	11.74	9.49	11.55	11.72	18.37	23.32	4.15	10.54	13.80	9.96
FR	34.72	38.42	33.49	39.27	41.23	43.10	44.55	39.03	37.17	31.94	38.23	40.41	39.52	41.19	37.16	38.18	34.75	37.43	38.22	37.39	39.80

Figure 6. Accuracy assessment chart with validation kappa for three ML algorithms, RF—SVM—CART, where, OA: overall accuracy, K: kappa.

dedicated to agriculture in Sahiwal was approximately 2510.40 square kilometers in 1990, with a modest growth observed in 1995. The CL area reached its highest point in 2002, measuring 2667.15 sq. km, and fluctuated in the following years, ultimately decreasing to 2601.10 sq. km by 2022.

3.2. Temporal cropland pattern transformation

This study observed variations in the area of cultivated land in Sahiwal across certain periods, measured in square kilometers (sq. km) and acres. Between 1990 and 1995, the cropland declined by 104.74 square kilometers, which is equivalent to 25,881.78 acres. However, it was consistent with 594,449.70 acres and showed a gain of 143.65 sq. km

as 35,496.63 acres during the same era. Subsequent intervals showed similar patterns, with oscillations in the agricultural areas. From 1995 to 2000, there was a loss of 19,093.80 acres, followed by a rise of 48,212.66 acres. The aforementioned time frames of 2000–2009, 2009–2013, 2013–2018, and 2018–2022 consistently demonstrated trends that indicated significant fluctuations in Sahiwal's cropland area. The cropland changes from 1990 to 2022 provide an overview of the total changes in the cropland area for the entire period. It indicates a net rise of 201.33 sq. km (49,749.65 acres) and a consistency of land on 2309.07 sq. km (570,582.69 acres) with a crop pattern shift or increase of 72162.07 acres. This comprehensive analysis offers useful insights into the changing patterns of croplands in Sahiwal over time (Figure 7).

This analysis provides a more detailed view of the changes in agricultural land. In addition, geographical analysis revealed the conversion of cropland into different types of land use, providing useful information for the planning and control of land use. The 8.01% cropland transformation to built-up and other land use was also observed from 1990 to 2022, the total area of cropland converted into built-up and other LU up to 15108.06 and 34641.65 acres, respectively. In the temporal observation from 1990 to 1995, 1995 to 2000, 2000 to 2009, 2009 to 2014, 2014 to 2018, 2018 to 2022 it was converted into built-up by 883.98, 780.85, 1479.84, 1512.28, 1821.88,
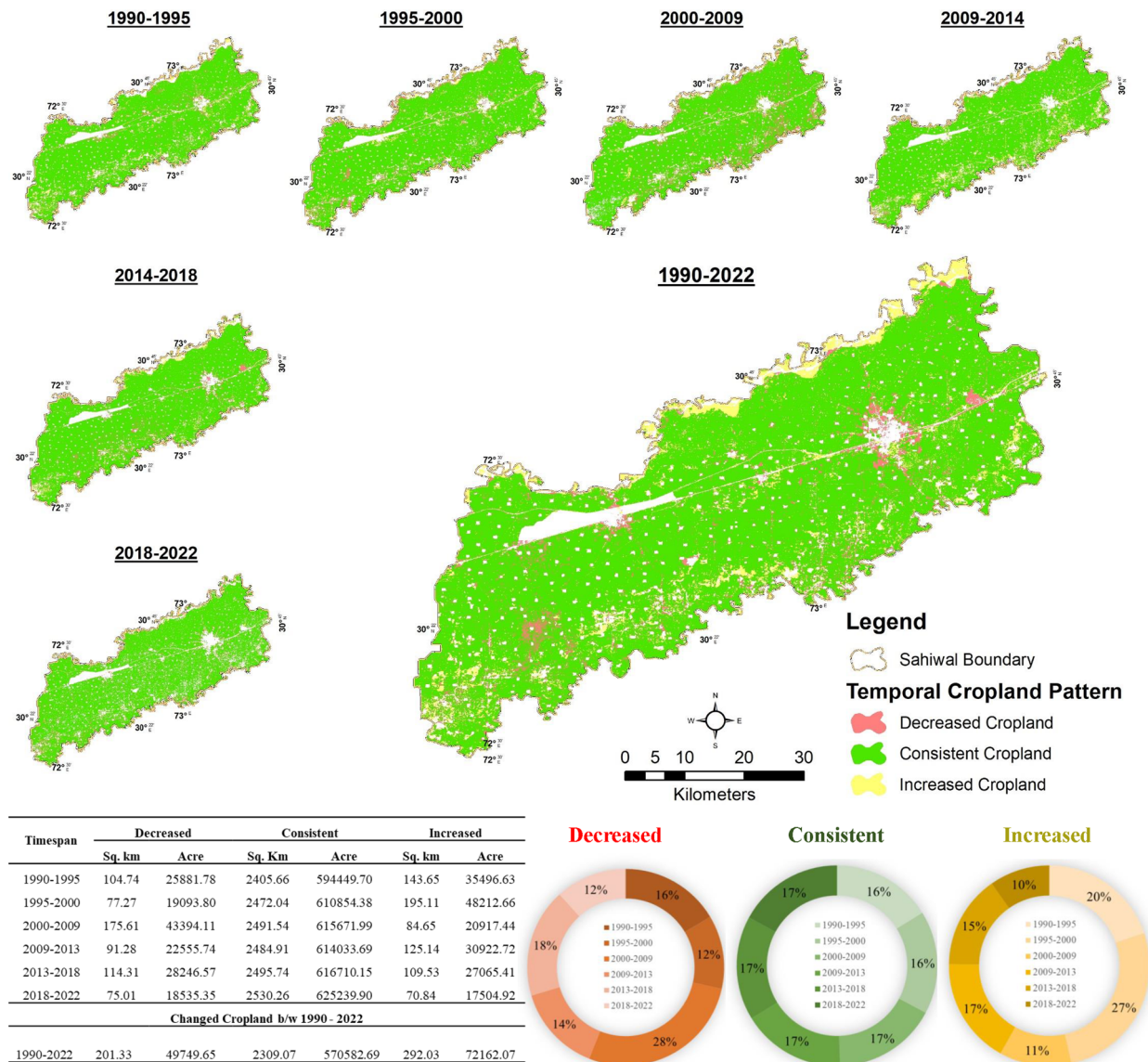
Timespan	Decreased		Consistent		Increased	
	Sq. km	Acre	Sq. Km	Acre	Sq. km	Acre
1990-1995	104.74	25881.78	2405.66	594449.70	143.65	35496.63
1995-2000	77.27	19093.80	2472.04	610854.38	195.11	48212.66
2000-2009	175.61	43394.11	2491.54	615671.99	84.65	20917.44
2009-2013	91.28	22555.74	2484.91	614033.69	125.14	30922.72
2013-2018	114.31	28246.57	2495.74	616710.15	109.53	27065.41
2018-2022	75.01	18535.35	2530.26	625239.90	70.84	17504.92
Changed Cropland b/w 1990 - 2022						
1990-2022	201.33	49749.65	2309.07	570582.69	292.03	72162.07

Figure 7. Temporal cropland pattern shifts with gain-loss in CL area from 1990 to 2022.

and 1949.66 acres, respectively. Whereas 24,997.14, 18312.95, 41988.08, 21043.46, 26425.41, and 16585.69 acres area were converted into other land uses in the observed time span temporally (Figure 8).

3.3. Cropland variations on LST and spectral indices

The dataset included a series of satellite-derived indices and LST measurements for Sahiwal over a span of seven years. NDVI, EVI, SAVI, MNDWI, BSI, and LST were calculated, and temporal patterns were observed using temporal Landsat satellite data (Table 5). NDVI and EVI displayed variations in vegetation vitality, whereas SAVI, MNDWI, and BSI emphasized alterations in soil and water dynamics. Furthermore, LST measurements depict fluctuations

in surface temperature over time. In 2022, NDVI varies between -0.02 and 0.75, which signifies changes in the health of vegetation. In Figure 9, insight observation shows cropland development and degradation patterns, as in the a and b areas along with the river, agricultural activity increased, which did not exist in 1990. Compared to the outputs of Region B, the cropland area was occupied by other land uses, such as built-up, barren, and fish farms. Their behavior is shown in the observed index categories, which exhibit a temporal transformation. On the other hand, the LST reported from 25.99 °C to 37.94 °C, signifying differences in LST (Figure 10).

The heat-map matrix shows how the cropland confronted the LST and vegetation and non-vegetation index variations over the observed period with
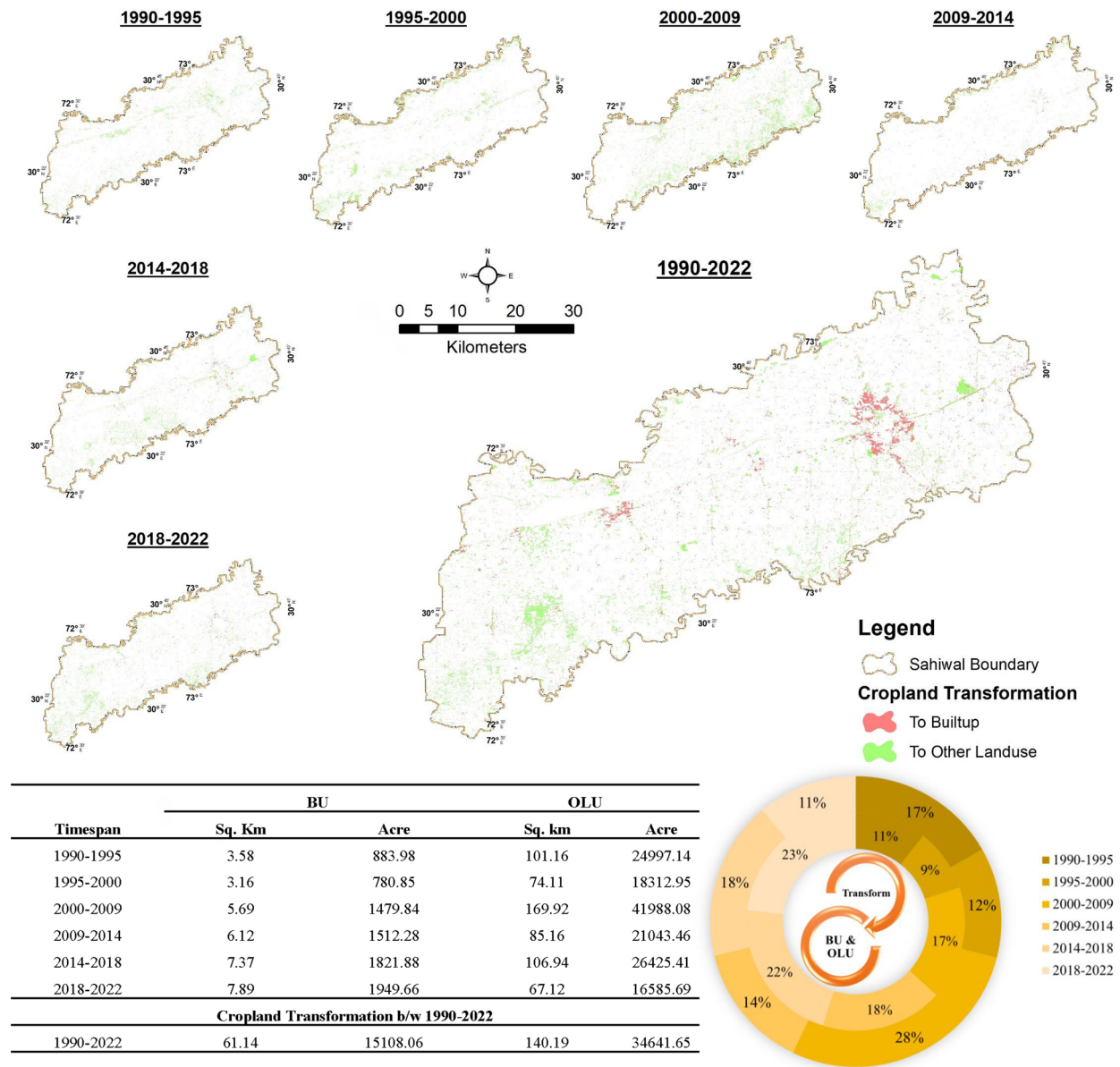
Figure 8. Cropland transformation to built-up and other land use classes from 1990 to 2022.

Table 5. Satellite derived indices annual temporal deviations with minimum and maximum ranges.

Years	NDVI		EVI		SAVI		MNDWI		BSI	
	Min	Max	Min	Max	Min	Max	Min	Max	Min	Max
2022	−0.02	0.75	−0.02	0.62	−0.01	0.57	−0.51	0.43	−0.29	0.25
2018	−0.05	0.69	−0.01	0.50	−0.06	0.66	−0.32	0.43	−0.22	0.18
2014	−0.15	0.72	−0.04	0.59	−0.05	0.55	−0.30	0.47	−0.32	0.20
2009	−0.13	0.64	−0.12	0.76	−0.09	0.64	−0.27	0.45	−0.28	0.23
2000	−0.19	0.64	−0.10	0.63	−0.11	0.58	−0.28	0.43	−0.26	0.16
1995	−0.17	0.68	−0.13	0.68	−0.24	0.95	−0.36	0.57	−0.30	0.18
1990	−0.28	0.72	−0.15	0.88	−0.16	0.62	−0.30	0.51	−0.29	0.17

interesting patterns (Figure 11). Significantly, there was a negative association between the LST and NDVI, EVI, and SAVI. This indicates that the cropland area is rich in crop health and soil fertility because lower temperatures are associated with more robust vegetation (Hussain et al., 2022; Marzban et al., 2018).

3.4. Wheat demand and supply—geographical indicators

3.4.1. Wheat acreages grown area

By visually interpreting the classified outcomes and NDVI profiles, the results showed variation in
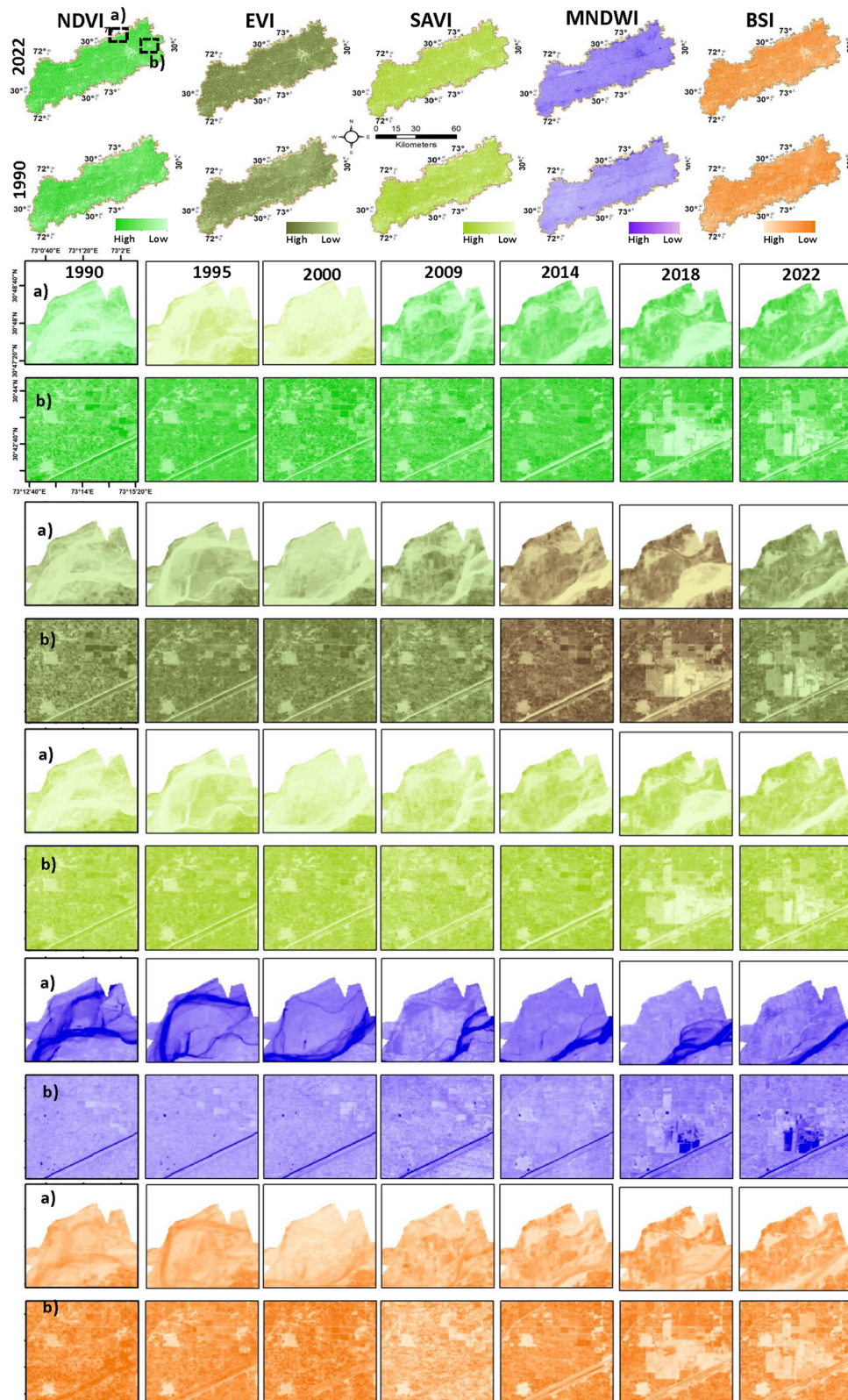
Figure 9. Satellite derived indices temporal behavior to analyses the rate of change and pattern shift of cropland from 1990 to 2022, region a and b presenting gain and loss in cropland areas.

temporal wheat, which was visualized by thorough analysis (Figure 12). The result is an all-encompassing map that depicts the spatial patterns of winter wheat farming in Sahiwal, providing vital knowledge for the temporal monitoring and control of agriculture, even with minimal resources (Figure 13).
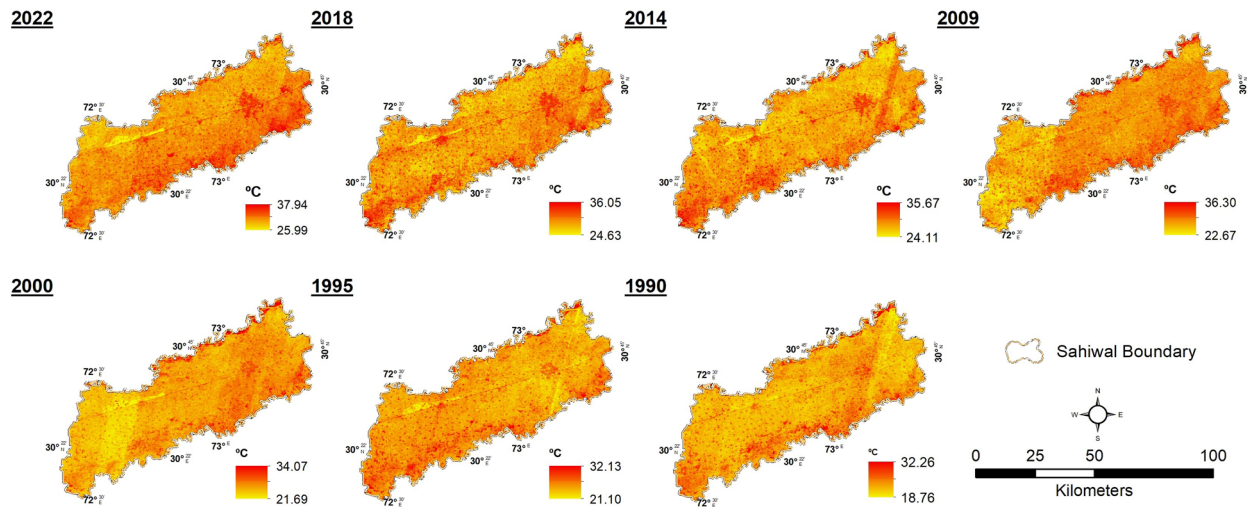
Figure 10. Land surface temperature temporal behavior.
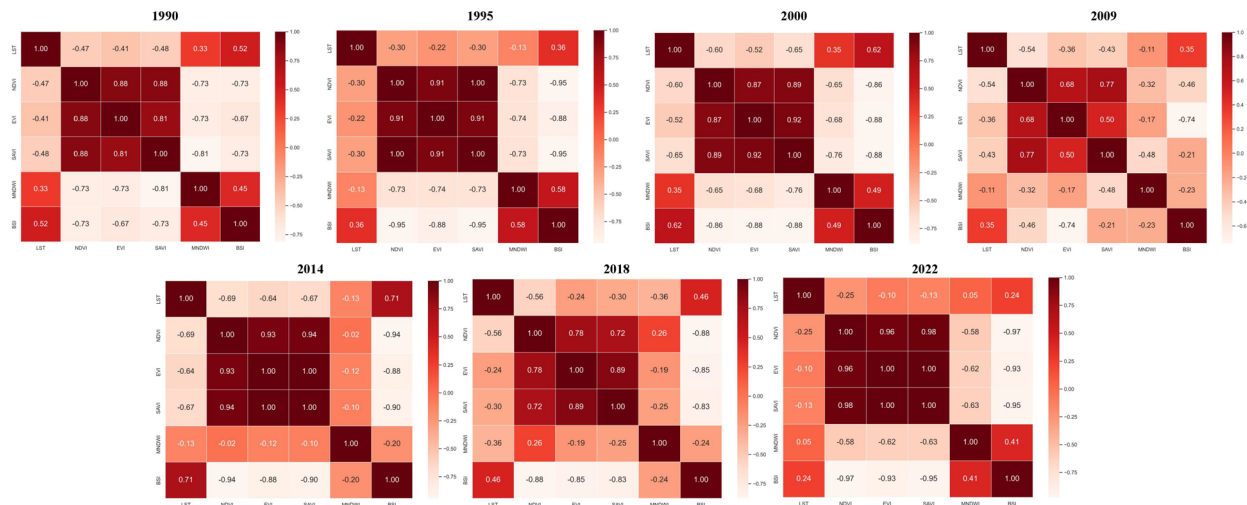

Figure 11. Correlation assessment using heat-map matrix LST and vegetation and non-vegetation indices on cropland area.

The results showed that wheat-grown areas have been reduced because of the cultivation of maize instead of wheat practices, as shown in Table 6. The classified and statistical areas of wheat will decrease by 2022. The RF results showed that the area of wheat was 392,383 acres in 1990, which was reduced to 274,264 acres by 2022. In comparison to statistical data from the agricultural department, the reported winter maize-grown area in 2009 was 45,600 acres which rapidly increased to 126000 acres by 2022.

In the wheat-grown area, a possible decrease of 28% has been noticed in 2022. Whereas the overall accuracy for the temporal wheat-grown area was estimated in the confusion matrix process and it observed that 96.17%, 95.21%, 93.33%, 94.42%, 95.84%, 92.79%, and 91.87% for the years 2022, 2018, 2014, 2009, 2000, 1995, and 1990, respectively.

3.4.2. Predictive population growth and patterns

Urbanization is an unavoidable outcome of economic advancement, resulting in a substantial increase in the urban population and demand for residential facilities (X. Q. Zhang, 2016). The exponential growth model predicts that Sahiwal's population will experience a substantial increase, reaching an estimated 3,347,799 by 2030 (Figure 14). The forecast, based on the model, shows a significant increase compared with earlier census data of 2,881,811 (2023), 2,513,011 (2017), 1,843,194 (1998), and 1,281,526 (1981). The model forecasts indicate a persistently rising trajectory, highlighting the region's demographic vitality. The high R-squared value of 0.97 indicates that BL has a strong correlation with the observed population statistics in Sahiwal. The high degree of connection between the model's forecasts and the actual population data significantly strengthens the reliability of the projections,
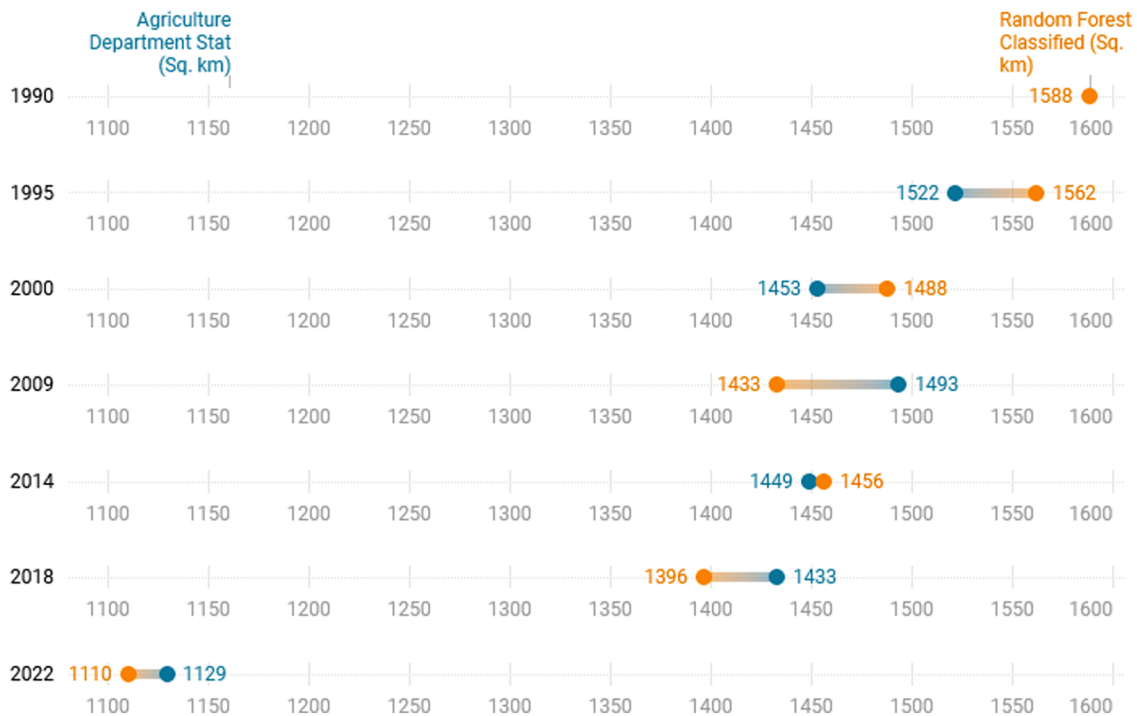
Figure 12. Comparison chart of remote sensing calculation with claimed statistics by Agriculture Department, Government Officials in sq. km.

hence strengthening confidence in the predicted population of 3,347,799 by the year 2030, with an increase of 112% as compared to 1990.

The LandScan data also illustrate a temporal rise in the population pattern of Sahiwal from 2000 to 2022 (Figure 15). LandScan population data provide a detailed and thorough representation of the spatial and temporal distribution of people in Sahiwal. The sustained increase in population during this timeframe indicates a significant change in population structure, possibly driven by causes such as urbanization, economic progress, or patterns of migration.

3.4.3. Socio-economic transformation—threaten to food security

Socio-economic Table 7 offers a thorough summary of wheat cultivation, agricultural productivity, and the corresponding socio-economic variables over several years, where a wheat area has varied in the observed years, showing a dramatic decline throughout the years and reaching 279,000 acres in 2022. The crop chlorophyll observed presents the average NDVI values, which indicate the overall health and vitality of the wheat crops throughout their growth season, and the highest mean value was recorded in 1995. A greater NDVI value often indicates more robust vegetation than a low NDVI value. Table 7 provides the essential metrics for wheat production, such as wheat required, yield, production, and per

capita availability and surplus. These statistics illustrate the per capita demand, production, and accessibility of wheat and provide insights into the food security state of the region (Table 7). The surplus column displays the excess amount of wheat available above the per capita requirement. This column demonstrates the potential for local sustenance, as well as the surplus that can be used for trade or storage purposes because Punjab Province is rich in cropland and wheat productivity. It has decreased from 116.41 to 12.51 kgs per capita per head up to 2022 which is alarming (Figure 16).

This socio-economic Table 7 is an excessive resource for comprehending the interplay between wheat output, population growth, and food security. The socioeconomic chart illustrates the complex interplay between population dynamics, wheat output, and per capita availability, emphasizing the difficulties and consequences of food security in Sahiwal.

The results of our method using the concept of 2SFCA (Zeng et al., 2023) with the defined catchment area, where the wheat accessibility ratio showed high and low demand for the year 2022. A value of less than 1 indicated a low accessibility ratio (Bell et al., 2013) resulting in high demand but less availability of wheat, and a value greater than 1 showed a balanced and high availability of wheat (Figure 17). This integrated method for food demand and consumption
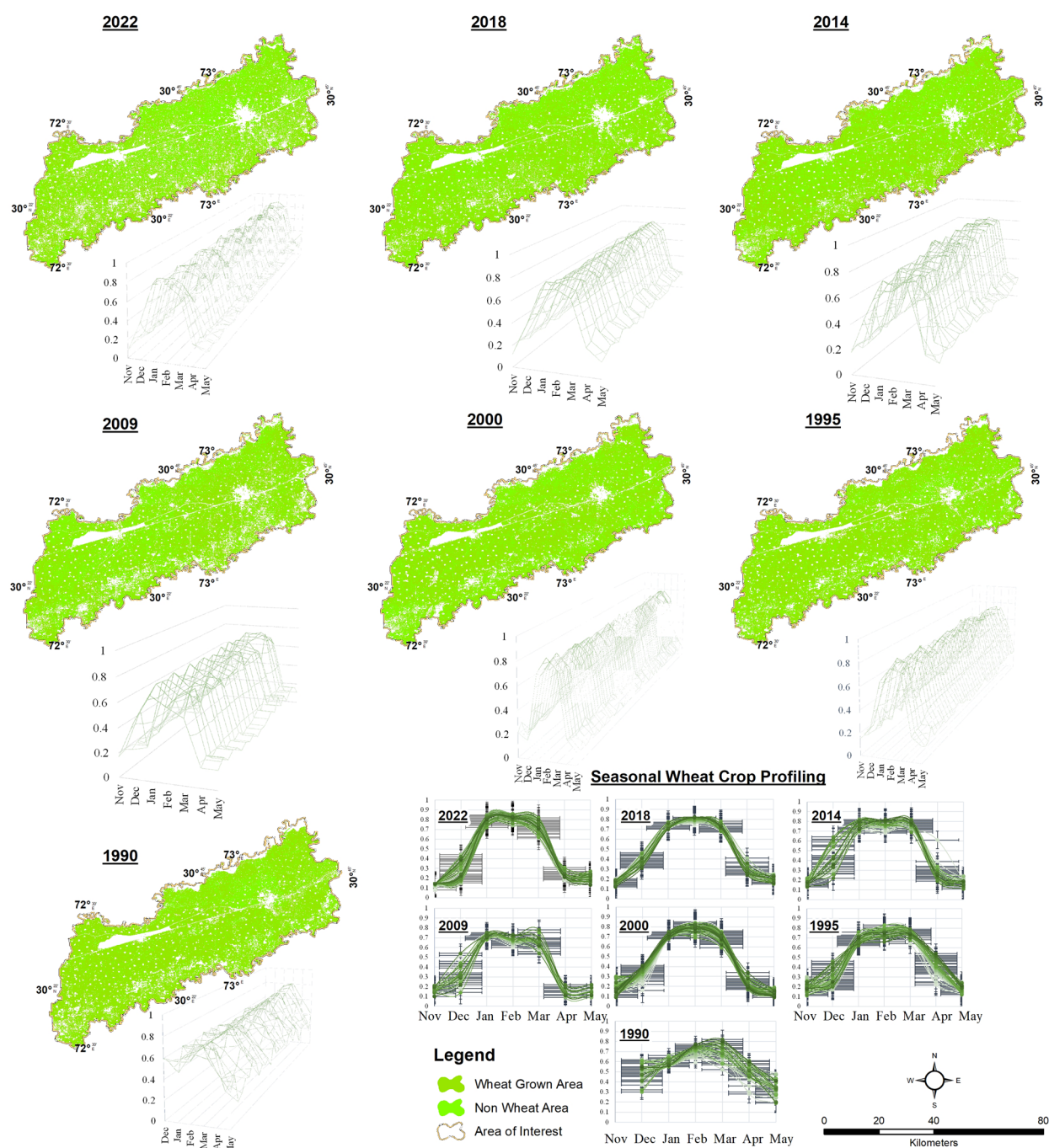
Figure 13. Wheat grown area results using NDVI profiling and supervised ML classification by wheat seasonal behavior observations.

Table 6. Temporal cropland and wheat grown area comparing of remote sensing and CRS stats.

	Remotely sensed—classified				Agriculture department stat	
	Cropland area—RF		Wheat area—RF		Wheat area—CRS	
Years	Sq. km	Acre	Sq. km	Acre	Sq. km	Acre
2022	2601.10	642744.82	1109.9	274,264	1,129.1	279,000
2018	2605.27	643775.24	1396.4	345,071	1,432.6	354,000
2014	2610.05	644956.41	1456.1	359,804	1,448.8	358,000
2009	2576.19	636589.43	1432.7	354,030	1,493.3	369,000
2000	2667.15	659066.10	1487.7	367,621	1,452.8	359,000
1995	2549.31	629947.25	1561.8	385,934	1,521.6	376,000
1990	2510.40	620332.39	1587.9	392,383	–	–

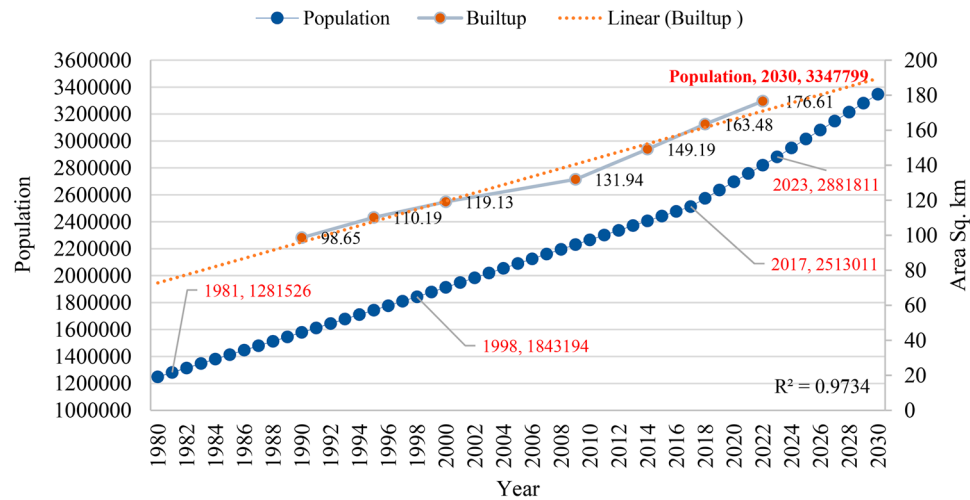CRS: Crop-reporting services, agriculture department.

Figure 14. Population dynamic graph from 1980 to 2023 with projected population till 2030 and temporal increase in built-up from 1990 till 2022 in sq. km ($r^2 = 0.97$).
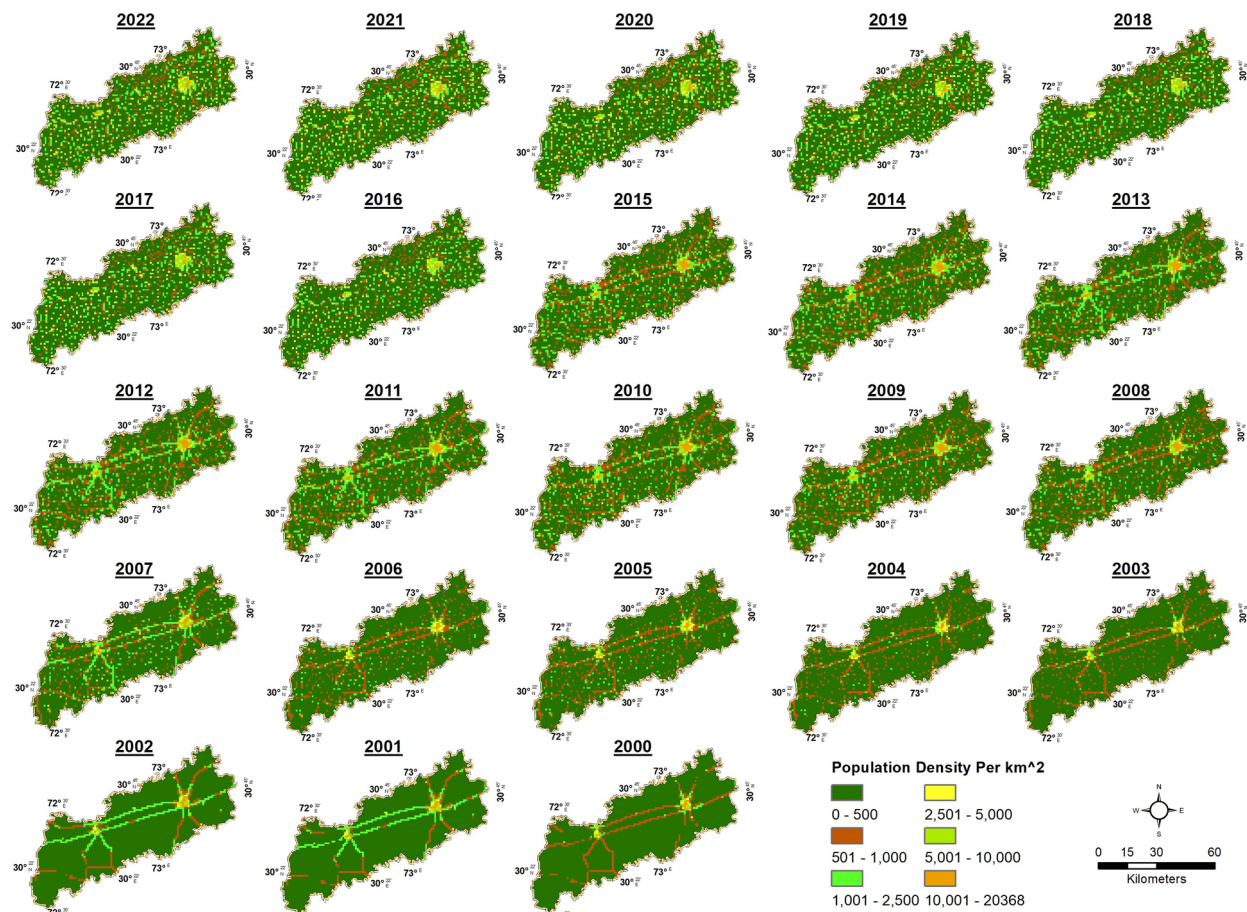

Figure 15. Geographical representation of population dynamics temporal pattern with increasing population trends using LandScan population density data.

has a significant influence on precision agriculture and sustainable farming to overcome food security issues. However, this research has some limitations regarding the availability and accuracy of satellite data, as well as socio-economic factors that require significant computational resources.

Table 7. Socioeconomic development under wheat per capita requirement from a past-present-future perspective threatens food security.

Years	Wheat grown area crs/classified		Mean LST wheat season	Crop health wheat season	POP	Wheat required		Production		Per capita availability & surplus, kgs	
	Acres	Sq. km	°C	Mean NDVI	Count	Kgs	Tons	Kgs	Tons	Availability	Surplus
2022	279,000	1,129.1	30.39	0.48	2,820,344	349,722,656	349,723	385,000,000	385,000	136.5	12.51
2018	354,000	1,432.6	30.58	0.43	2,574,478	319,235,272	319,235	497,000,000	497,000	193.0	69.05
2014	358,000	1,448.8	28.33	0.45	2,407,250	298,499,000	298,499	464,000,000	464,000	192.8	68.75
2009	369,000	1,493.3	26.74	0.46	2,230,983	276,641,892	276,642	460,000,000	460,000	206.2	82.19
2000	359,000	1,452.8	23.78	0.47	1,913,701	237,298,924	237,299	478,000,000	478,000	249.8	125.78
1995	376,000	1,521.6	23.7	0.50	1,744,076	216,265,424	216,265	419,000,000	419,000	240.4	116.41
1990	392,383	1587.9	22.64	0.40	1,578,880	195,781,120	195,781	–	–	–	–
2030					3,347,799	415,127,076	415,127				

*Annual per capita consumption (kg) = 124.
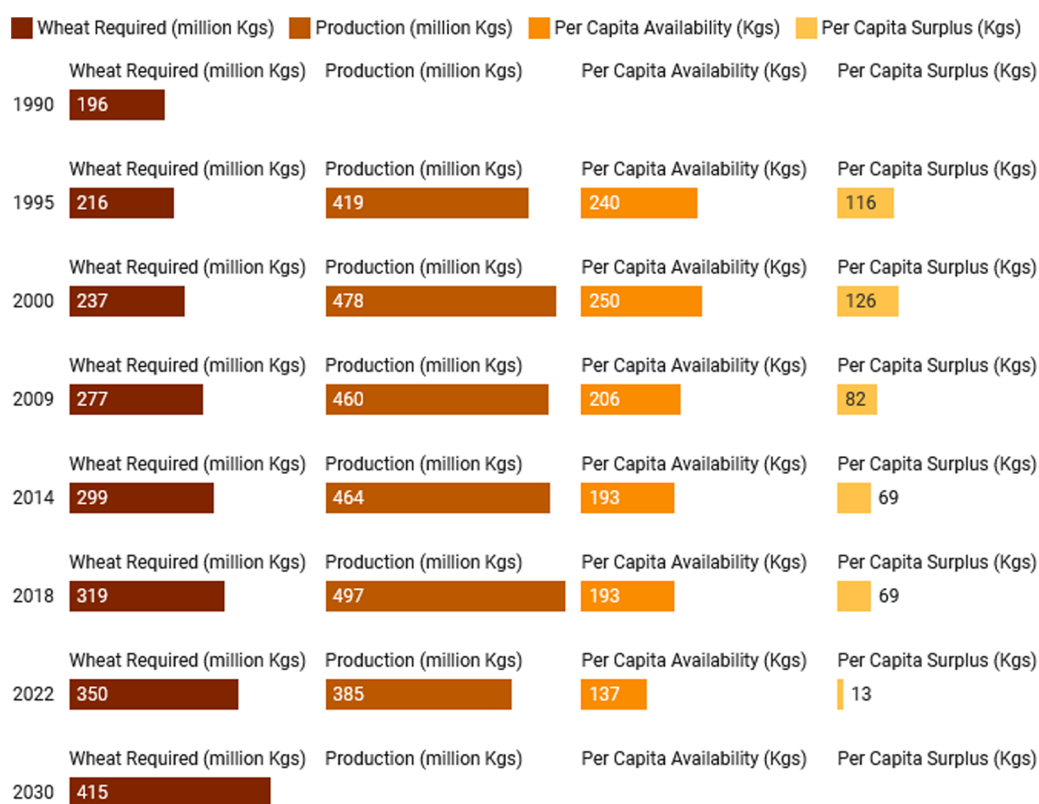
Figure 16. Wheat crop requirement, production, availability, and surplus observed statistical chart in kilograms.

4. Discussion

The study period involved quantifying changes in cropland areas, including their consistency, gain, and loss. This thorough examination illuminates the complex patterns of land cover changes in Sahiwal, offering a significant understanding of the transitions between cropland, urban areas, and other land use categories during the observed periods. The integration of remote sensing, machine learning and socio-economic data analysis highlights significant challenges and scenarios for agriculture productivity and food security in the region with rapid urbanization. The analysis reveals intricate patterns of transformation of agricultural land into urban expansion and other land uses across time, providing valuable insights into the evolving environment. From 1990 to 2022, approximately 8.01% of Sahiwal's cropland was converted to non-agricultural land. The expansion of urban areas indicates a rise in urbanization, population concentration, and infrastructure development, emphasizing the significant changes in cropland for non-agricultural activities in the region. This trend is consistent with global patterns where
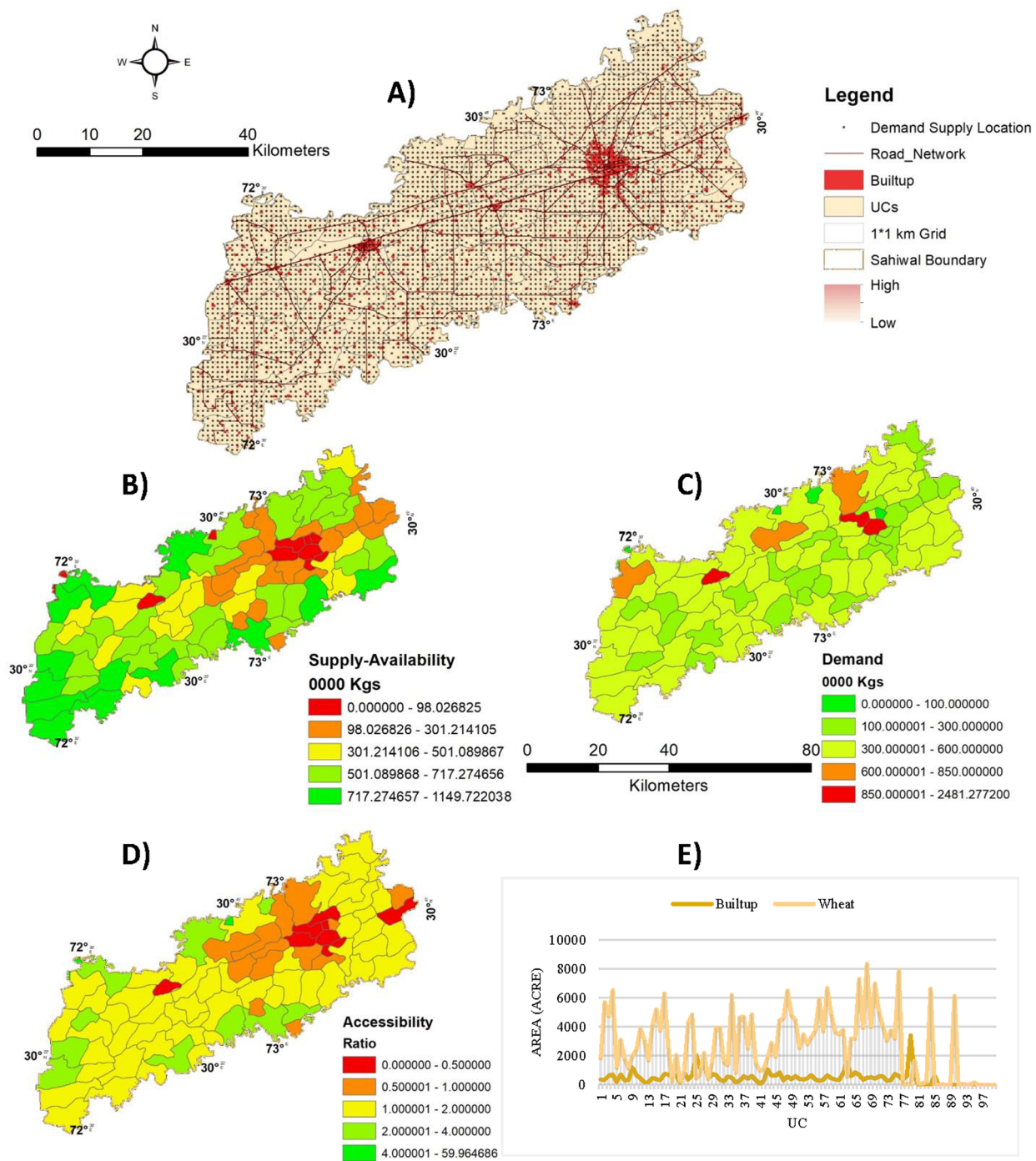
Figure 17. Spatial distribution of wheat accessibility identified (A) acquired data, (B) spatial availability of wheat in Kgs, (C) demand per UC in Kgs, (D) identified accessibility ratio, and (E) built-up and wheat grown area evaluation in each UC.

urban expansion increasing pressure on cultivable land, thereby reducing agricultural productivity and challenging food security (He et al., 2017; Rahimi et al., 2021). The high classification accuracy achieved through machine learning approach, particularly with the RF algorithm. RF enhances accuracy without overfitting, making it a valuable tool for temporal land-cover studies (Zhao et al., 2024), while the

highest achieved accuracy was 95.22% in this study. Additional prominent land-cover categories, including BU, BL, VE, WT, and FR, revealed diverse patterns of change throughout the study period. There is an inverse relationship between the vegetation indices and surface temperature (Sohail et al., 2023), with little variation in the temporal observation due to crop pattern changes.

The use of satellite indices such as NDVI, SAVI, BSI, MNDWI, and EVI in this study provided significant observations of vegetation health and soil conditions, which align with the general advantages these indices offer in assessing cropland dynamics and soil moisture across temporal spans (Hussain et al., 2023; Raza et al., 2024). However, there are positive connections between LST, MNDWI, and BSI, which indicates a possible link between higher temperatures and non-vegetation indices. Moreover, a precise examination of the negative associations between LST and MNDWI in 1995, 2009, and 2018 shows temporal variations in the interaction between temperature cropland behavior over time. This thorough heat map study offers useful insights into the many relationships that influence the agricultural environment and its response to climatic factors. This extensive dataset offers a detailed comprehension of time-based changes in Sahiwal's land cover and environmental circumstances. However, an increasing trend was reported in the LST, and an inverse relationship exists with the vegetation index, including NDVI (Marzban et al., 2018). Population expansion in Sahiwal has significant consequences for urban development, infrastructure planning, and the necessity of implementing sustainable practices to support the growing population. Temporal growth is examined along with other socioeconomic and environmental factors and can offer useful insights into the dynamics of the region in this research. Population growth was also observed in the LandScan spatial pattern, which was low in 2000, but in 2022, the whole district faced high population clusters. The results also revealed that the presented scenario depicts the development of urban land in Sahiwal during the analyzed years. The assembled cluster presented a growth scenario, as clearly observed in the LandScan population density data. The population showed an increasing trend, which may also affect crop cultivation practices and cause temperature fluctuations (Hou et al., 2021; Sohail et al., 2023).

The wheat-grown area has been decreasing as the demand for wheat has risen day by day compared to 1990. The reported decrease of 28% in wheat-cultivated areas, along with a significant surge in population (79% between 1990 and 2022 and projected to exceed 112% by 2030), demonstrates how socio-economic growth strains food production and security systems. In Pakistan, high pressure also exists in Punjab Province because it is a fertile and agriculture-rich province (Tariq et al., 2023). Additionally, it supplies wheat to neighboring provinces, including Baluchistan and KPK, which have less suitable areas

for wheat crops (Tahir & Khaliq, 2018). Therefore, it is necessary to meet the needs of the entire country. The surplus needs to increase in line with the population, but it is decreasing due to the growing population, which poses a threat to food security (S. Yang et al., 2023). The socio-economic analysis revealed that Sahiwal's rapid population growth, projected to surpass 3.3 million by 2030, will continue to drive wheat demand. It is necessary to fulfil the needs of the entire country; the surplus can increase as per the population, but it reduces as an increasing trend in population, which becomes a threat to food security. The 2SFCA model in this study provided spatial insights into wheat demand and accessibility. Previous studies demonstrate the utility of the 2SFCA model in mapping food accessibility and addressing supply-demand gaps with other utility assessments (X. Chen, 2019; X. Chen & Jia, 2019; Bell et al., 2013). The findings emphasize the challenges posed by population growth in guaranteeing food security, highlighting the need for proactive implications. On the other hand, wheat crop production with other parameters is nearly stagnant from 2000 observations, but the demand is increasing rapidly and the wheat grown area is decreasing as well. The year 2030 depicts a projected scenario forecasting a substantial rise in population and the corresponding implications for wheat farming and accessibility. The results also revealed that the availability of wheat decreased by two factors due to land use, land cover, and crop pattern shift (cultivation of wheat crop reduced by maize). Examination of changes in crops revealed substantial modifications in agricultural trends, distinguishing between regions experiencing expansion, contraction, and consistency (Hou et al., 2021; Hussain et al., 2022). This study's approach supports the United Nations' Sustainable Development Goal 2 (Zero Hunger) by offering a robust framework for food security assessment in rapidly urbanizing regions. The examined effects of land dynamics on local communities, livelihoods, and the overall economy, revealing the complex relationship between these factors, show that a consistent decrease in per capita availability is a serious threat to food security. The results offer a crucial direction for resource allocation and urban planning to handle changing environmental and socioeconomic issues for food sustainability.

5. Conclusion

This study improves agricultural monitoring techniques and land management, and provides important information for the formulation of policies

affecting sustainable development. The integration of remote sensing and socioeconomic data with demographic and statistical information increases the reliability of the study, especially for the evaluation of food security-related issues. This study employed a thorough approach to comprehend the complex dynamics of Sahiwal's landscape development. Through a comparative application of machine learning techniques, RF is the most efficient model for categorizing land cover, including cropland, with the observed highest accuracy of 95.22%. In addition, the use of indicators collected from satellites allowed for a thorough understanding of the temporal trends and correlation patterns in the study area. This investigation primarily examined the transformation of agricultural land into developed areas and other land uses, providing significant observations on the evolving trends of urbanization in 2022. The 15108.06 acres and 34637.52 acres area of cropland change into built-up and other land use, respectively. The wheat grown area achieved the highest accuracy of 96.17% in the results of phenological and spectroscopic based modeling using CLE-WAAM methodology. However, the study on socio-economic effects highlighted the significant consequences of changes in cropland, especially for wheat crops as of 2022. A total of 349,722,656 kg of wheat is required, which will increase to 415,127,076 kg by 2030. By contrast, the proposed methodology interactively supports linked factors that are helpful for the investigation of the 2SFCA model with integrated data. The accessibility ratio of demand and supply from <1 to 0 indicated high demand and low supply due to the flux of urbanization. This research showed the capacity for regional self-sufficiency, as well as the excess that may be utilized for trade or storage due to the abundant cropland and high wheat output in the Punjab provinces. On the other hand, the wheat crop's yield, production, and area, along with other parameters, have remained relatively unchanged since 2000, while demand has experienced rapid growth. This integrated and improved methodology for land management, population analysis, and food security investigation will be beneficial for future analytical observations. For a better understanding and implication of the SDG goal (zero hunger), this methodology will help in the spatial pattern assessment of food consumption and supply in any region using open access data in a time-efficient manner. This highlights the significance of meticulous strategies and interventions to guarantee sustainable and ecologically conscious progress regarding this issue. This study provides a comprehensive framework that assists decision makers and scholars engaged in sustainable land management and agricultural planning.

Authors' contributions

Danish Raza: Conceptualization, field survey, data acquisition, methodology, analysis, investigation, prepared original draft, and research. Hong Shu and Hong Fan supervised the study and obtained funding. Muhsan Ehsan: review and initial draft improvement; Kamal Abdelrahman: review and funding; Hasnat Aslam, Abdul Quddoos, and Rana Waqar Aslam: data acquisition and draft improvement. Majid Nazeer, data gathering, and improvement of the initial draft. Mohammed S. Fnais and Azeem Sardar review to improve the initial draft. All the authors have proofread the manuscript.

Disclosure statement

The authors declare no conflict of interest.

Future work

This approach combines data integration, geographic analysis, and socioeconomic variables to create a thorough understanding of the factors affecting wheat production and accessibility in the area. The robustness of this approach will also contribute to a broader perspective, and it will be applied on a global scale, which is the main theme in future perspective research under the sustainable development goals of the United Nations.

About the authors

Danish Raza is pursuing a PhD in Cartography and Geographic Information Engineering at the State Key Laboratory of Information Engineering in Surveying, Mapping, and Remote Sensing, Wuhan University, China. He is a recipient of a fully funded scholarship for his doctoral studies. His research integrates multi-sensor remote sensing data, spectroscopy, agro-ecological modeling, and geospatial analysis to address challenges in crop identification, agricultural assessments incorporating socio-economic factors, and land use evaluation. He has published several research articles across diverse fields, including remote sensing applications, geospatial modeling, environmental monitoring, sustainable development, and their implications for policy-making and decision support systems.

Hong Shu is a full professor of Geoinformatics at the State Key Laboratory of Information Engineering in Surveying, Mapping, and Remote Sensing, Wuhan University, China. He completed his PhD in Photogrammetry and Remote Sensing from Wuhan Technical University of Surveying and Mapping, China. He has diverse experience in global and local scientific investigation in academia and scientific projects. He specializes in spatiotemporal computation and geospatial information technology, and has published around 100 research articles.

Muhsan Ehsan received his PhD in Exploration Geophysics from China University of Geosciences (Wuhan) in 2016. He obtained his MSc degree from Quaid-i-Azam University Islamabad in 2011. Now he is working as a Senior Associate professor at the Department of Earth and Environmental Sciences, Bahria University Islamabad, PK. He has vast experience in researching geothermal, LULC, machine learning, deep learning, source rock evaluation, and water sources management. He has successfully delivered multiple research-based projects with grants issued by the Higher Education Commission of Pakistan. He has published more than 70 research articles, and their research outcomes have been recognized and presented in several international forums.

Hong Fan was born in Hunan, China. She received the B.S. and M.S. degrees in computer science, in 1988 and 1991, respectively, and the Ph.D. degree in GIS and remote sensing from Wuhan University, China, in 2001, where she is currently a Professor and the Ph.D. Supervisor. She is also a Geographic Information System and Remote Sensing expert. She has been involved in teaching and research in cartography & geographic information system and remote sensing for a long time. Her research interests include smart geographic information service, spatial-temporal big data mining, agriculture, and environmental remote sensing monitoring.

Kamal Abdelrahman graduated from the Geology Department, Zagazig University, Egypt, in May 1990 with a Very Good grade. He got his M.Sc. and PhD in applied Geophysics from Zagazig University, Egypt. He has worked as a full professor at the Department of Geology and Geophysics, King Saud University, Riyadh, Saudi Arabia, since 2011. He published over 240 original articles in peer-reviewed Journals and 53 conference abstracts. He is a reviewer in several journals.

Hasnat Aslam, PhD Scholar at College of Agriculture and Natural Resources, University of Nebraska-Lincoln, Lincoln, Nebraska, United States of America (USA), USA. He is currently serving as a GIS Specialist at the National Drought Mitigation Center, Nebraska Lincoln, Lincoln, USA as well. Before joining UNL, Hasnat worked for the Punjab Agriculture Department as a GIS Analyst. His research interests include data analytics, spatial analysis, machine learning, agriculture monitoring and hydraulic modeling.

Abdul Quddoos received the MS degree in Photogrammetry & Remote Sensing from the State Key Laboratory of Information Engineering in Surveying, Mapping, and Remote Sensing, Wuhan University, Wuhan, China in 2024. His research interests are deeply rooted in utilizing remote sensing and GIS technologies to tackle environmental and geographical challenges, with a particular focus on climate change impacts on agriculture and the application of remote sensing in disaster management. Abdul has distinguished himself in academia and professional circles through his contributions to scientific journals and active participation in international forums.

Rana Waqar Aslam is an esteemed researcher at the State Key Laboratory of Information Engineering in Surveying, Mapping, and Remote Sensing at Wuhan University, China. With a specialized focus on remote sensing, photogrammetry, and geographical information systems, Dr. Aslam has made significant contributions to the field through his research on multiple satellite data. His expertise extends across various satellite imaging technologies, including multispectral, hyperspectral, and SAR data processing. Dr. Aslam's professional journey in remote sensing and geospatial analysis has included roles that blend academic research with practical applications, enabling enhanced understanding and management of Earth's physical and cultural environments.

Majid Nazeer has earned his PhD from the Department of Land Surveying and Geo-Informatics (LSGI), The Hong Kong Polytechnic University (PolyU), Hong Kong during 2016. Currently, he is serving his alma mater (PolyU) as Research Assistant Professor. His research interests include applications of remote sensing in inland/coastal waters, agricultural crop yield estimation, vegetation health monitoring, atmospheric aerosols and atmospheric correction of satellite imagery and blue carbon sinks. His current research is on exploring the role of Blue Carbon sinks (i.e. Mangroves, marshes and seagrasses) in carbon sequestration through earth observation datasets.

Mohammed S. Fnais received his B.Sc. in Geophysics from the Faculty of Sciences - King Saud University in 1995. He got his M.Sc. in Applied Geophysics at the University of Tulsa – Oklahoma, United States, in 1999. He got his Ph.D. in Seismology - at the University of St. Louis – Missouri, United States in 2004. He worked as Professor of Seismology, Geology and Geophysics Department - College

of Science- King Saud University, Riyadh, Saudi Arabia. He has published 77 original articles in peer-reviewed journals.

Azeem Sardar is an Agro-Economist who earned his PhD in Economics from Government College University Faisalabad, Pakistan, in 2017. With over 12 years of experience, he specializes in agriculture, livestock, food security, climate-resilient agriculture, and spatial planning. Currently serving as Senior Program Manager (Agricultural Development) at Urban Unit Lahore and placed at the Institute of Agricultural and Resource Economics, University of Agriculture Faisalabad, he has contributed to transformative policy initiatives like Punjab Spatial Strategy (2047) and World Bank projects. His work includes 12 publications and extensive research supporting climate-resilient policy actions in Punjab, Pakistan.

ORCID

Danish Raza http://orcid.org/0000-0002-7623-3666
Kamal Abdelrahman http://orcid.org/0000-0002-9473-6769

Data availability statement

The supporting data used to generate the results are available upon reasonable request from the corresponding author.

References

Adam, E., Mutanga, O., Odindi, J., & Abdel-Rahman, E. M. (2014). Land-use/cover classification in a heterogeneous coastal landscape using rapideye imagery: Evaluating the performance of random forest and support vector machines classifiers. *International Journal of Remote Sensing*, 35(10), 3440–3458. https://doi.org/10.1080/01431161.2014.903435

Aeman, H., Shu, H., Abbas, S., Aisha, H., & Usman, M. (2023). Sinking delta: Quantifying the impacts of saltwater intrusion in the Indus Delta of Pakistan. *The Science of the Total Environment*, 880(July), 163356. https://doi.org/10.1016/j.scitotenv.2023.163356

Ahmad, N., Khan, S., Ehsan, M., Rehman, F. U., & Al-Shuhail, A. (2022). Estimating the total volume of running water bodies using geographic information system (GIS): A case study of Peshawar Basin (Pakistan). *Sustainability*, 14(7), 3754. https://doi.org/10.3390/su14073754

Akinyemi, F. O., Pontius, R. G., & Braimoh, A. K. (2016). Land Change Dynamics: Insights from Intensity Analysis Applied to an African Emerging City. *Journal of Spatial Science*, (June), 1–15. https://doi.org/10.1080/14498596.2016.1196624

Aloo, B. N., Makumba, B. A., & Mbega, E. R. (2019). The potential of Bacilli Rhizobacteria for sustainable crop production and environmental sustainability. *Microbiological Research*, 219(February), 26–39. https://doi.org/10.1016/j.micres.2018.10.011

Alshari, E. A., & Gawali, B. W. (2021). Development of classification system for LULC using remote sensing and GIS. *Global Transitions Proceedings*, 2(1), 8–17. https://doi.org/10.1016/j.gltp.2021.01.002

Amani, M., Ghorbanian, A., Ahmadi, S. A., Kakooei, M., Moghimi, A., Mirmazloumi, S. M., Moghaddam, S. H. A., Mahdavi, S., Ghahremanloo, M., Parsian, S., Wu, Q., & Brisco, B. (2020). Google earth engine cloud computing platform for remote sensing big data applications: A comprehensive review. *IEEE Journal of Selected Topics in Applied Earth Observations and Remote Sensing*, 13, 5326–5350. https://doi.org/10.1109/JSTARS.2020.3021052

Aslam, R. W., Shu, H., Javid, K., Pervaiz, S., Mustafa, F., Raza, D., Ahmed, B., Quddoos, A., Al-Ahmadi, S., & Hatamleh, W. A. (2024). Wetland identification through remote sensing: Insights into wetness, greenness, turbidity, temperature, and changing landscapes. *Big Data Research*, 35(February), 100416. https://doi.org/10.1016/j.bdr.2023.100416

Ayat, N. E., Cheriet, M., & Suen, C. Y. (2005). Automatic model selection for the optimization of SVM kernels. *Pattern Recognition*, 38(10), 1733–1745. https://doi.org/10.1016/j.patcog.2005.03.011

Bakker, V., Verburg, P. H., & van Vliet, J. (2021). Trade-offs between prosperity and urban land per capita in major world cities. *Geography and Sustainability*, 2(2), 134–138. https://doi.org/10.1016/j.geosus.2021.05.004

Ball, J. E., Anderson, D. T., & Chan, C. S. (2017). Comprehensive survey of deep learning in remote sensing: Theories, tools, and challenges for the community. *Journal of Applied Remote Sensing*, 11(04), 1. https://doi.org/10.1117/1.JRS.11.042609

Bell, S., Wilson, K., Bissonnette, L., & Shah, T. (2013). Access to primary health care: Does neighborhood of residence matter? *Annals of the Association of American Geographers*, 103(1), 85–105. https://doi.org/10.1080/00045608.2012.685050

Bouasria, A., Rahimi, A., El Mjiri, I., Namr, K. I., Ettachfini, E. M., & Bounif, M. (2021a). *Use of Remote Sensing Data to Estimate Sugar Beet Crop Yield in the Doukkala Irrigated Perimeter* [Paper presentation]. 2021 Third International Sustainability and Resilience Conference: Climate Change, In, 504–507. IEEE. https://doi.org/10.1109/IEEECONF53624.2021.9668059

Bouasria, A., Rahimi, A., El Mjiri, I., Namr, K. I., Ettachfini, E. M., & Bounif, M. (2021b). *Comparative Study between Two Methods of Crop Classification in the Irrigated Area of Sidi Bennour* [Paper presentation]. 2021 Third International Sustainability and Resilience Conference: Climate Change, In, 500–503. IEEE. https://doi.org/10.1109/IEEECONF53624.2021.9668069

Bounif, M., Bouasria, A., Rahimi, A., & El Mjiri, I. (2021). *Study of Agricultural Land Use Variability in Doukkala Irrigated Area between 1998 and 2020* [Paper presentation]. 2021 Third International Sustainability and Resilience Conference: Climate Change, In, 170–175. IEEE. https://doi.org/10.1109/IEEECONF53624.2021.9667965

Bouslihim, Y., John, K., Miftah, A., Azmi, R., Aboutayeb, R., Bouasria, A., Razouk, R., & Hssaini, L. (2024). The effect of covariates on soil organic matter and PH variability: A digital soil mapping approach using random forest model. *Annals of GIS*, 30(2), 215–232. https://doi.org/10.1080/19475683.2024.2309868

Breiman, L. (2001). Random forests. *Machine Learning*, 45(1), 5–32. https://doi.org/10.1023/A:1010933404324

Cao, R., Chen, Y., Shen, M., Chen, J., Zhou, J., Wang, C., & Yang, W. (2018). A simple method to improve the quality of NDVI time-series data by integrating spatiotemporal information with the Savitzky-Golay filter. *Remote*

Sensing of Environment, 217(November), 244–257. https://doi.org/10.1016/j.rse.2018.08.022

Chen, C., Wang, L., Yang, G., Sun, W., & Song, Y. (2023). Mapping of ecological environment based on Google earth engine cloud computing platform and landsat long-term data: A case study of the Zhoushan Archipelago. Remote Sensing, 15(16), 4072. https://doi.org/10.3390/rs15164072

Chen, R.-C., Dewi, C., Huang, S.-W., & Caraka, R. E. (2020). Selecting critical features for data classification based on machine learning methods. Journal of Big Data, 7(1), 52. https://doi.org/10.1186/s40537-020-00327-4

Chen, X. (2019). Enhancing the two-step floating catchment area model for community food access mapping: Case of the supplemental nutrition assistance program. The Professional Geographer, 71(4), 668–680. https://doi.org/10.1080/00330124.2019.1578978

Chen, X., & Jia, P. (2019). A comparative analysis of accessibility measures by the two-step floating catchment area (2SFCA) method. International Journal of Geographical Information Science, 33(9), 1739–1758. https://doi.org/10.1080/13658816.2019.1591415

Cheng, X., Sun, Y., Zhang, W., Wang, Y., Cao, X., & Wang, Y. (2023). Application of deep learning in multitemporal remote sensing image classification. Remote Sensing, 15(15), 3859. https://doi.org/10.3390/rs15153859

Choubin, B., Darabi, H., Rahmati, O., Sajedi-Hosseini, F., & Kløve, B. (2018). River suspended sediment modelling using the CART Model: A comparative study of machine learning techniques. The Science of the Total Environment, 615(February), 272–281. https://doi.org/10.1016/j.scitotenv.2017.09.293

d., Silva, V. S., G., Salami, M. I. O. d., Silva, E. A., Silva, J. J., Monteiro Junior., & E., Alba. (2020). Methodological evaluation of vegetation indexes in land use and land cover (LULC) classification. Geology, Ecology, and Landscapes, 4(2), 159–169. https://doi.org/10.1080/24749508.2019.1608409

Derdouri, A., Wang, R., Murayama, Y., & Osaragi, T. (2021). Understanding the links between LULC changes and SUHI in cities: Insights from two-decadal studies (2001–2020). Remote Sensing, 13(18), 3654. https://doi.org/10.3390/rs13183654

Devkota, K. P., Bouasria, A., Devkota, M., & Nangia, V. (2024). Predicting wheat yield gap and its determinants combining remote sensing, machine learning, and survey approaches in rainfed Mediterranean regions of Morocco. European Journal of Agronomy, 158(August), 127195. https://doi.org/10.1016/j.eja.2024.127195

DeVries, B., Huang, C., Armston, J., Huang, W., Jones, J. W., & Lang, M. W. (2020). Rapid and robust monitoring of flood events using sentinel-1 and landsat data on the Google earth engine. Remote Sensing of Environment, 240(April), 111664. https://doi.org/10.1016/j.rse.2020.111664

Diem, P. K., Nguyen, C. T., Diem, N. K., Diep, N. T. H., Thao, P. T. B., Hong, T. G., & Phan, T. N. (2024). Remote sensing for urban heat island research: Progress, current issues, and perspectives. Remote Sensing Applications: Society and Environment, 33(January), 101081. https://doi.org/10.1016/j.rsase.2023.101081

Drummond, M. A., Auch, R. F., Karstensen, K. A., Sayler, K. L., Taylor, J. L., & Loveland, T. R. (2012). Land change variability and human–environment dynamics in the United States great plains. Land Use Policy, 29(3), 710–723. https://doi.org/10.1016/j.landusepol.2011.11.007

Duan, T., Chapman, S. C., Guo, Y., & Zheng, B. (2017). Dynamic monitoring of NDVI in wheat agronomy and breeding trials using an unmanned aerial vehicle. Field Crops Research, 210(August), 71–80. https://doi.org/10.1016/j.fcr.2017.05.025

Ehsan, M., Shabbir, H., Al-Quraishi, A. M. F., Al-Ansari, N., Ahmad, Z., Abdelrahman, K., Sohail, M. T., Manzoor, Z., Shafi, A., & Elbeltagi, A. (2024). Groundwater delineation for sustainable improvement and development aided by GIS, AHP, and MIF techniques. Applied Water Science, 14(2), 23. https://doi.org/10.1007/s13201-023-02065-3

El Mjiri, I., Rahimi, A., & Bouasria, A. (2021). Soil Artificialization Assessment by Using Time Series Remote Sensing Data (Case El Jadida) [Paper presentation].2021 Third International Sustainability and Resilience Conference: Climate Change, 452–455. IEEE. https://doi.org/10.1109/IEEECONF53624.2021.9667985

Erbek, F. S., Özkan, C., & Taberner, M. (2004). Comparison of maximum likelihood classification method with supervised artificial neural network algorithms for land use activities. International Journal of Remote Sensing, 25(9), 1733–1748. https://doi.org/10.1080/0143116031000150077

FAO. (2017). The future of food and agriculture—Trends and challenges. Food and Agriculture Organization of the United Nation.

Feizizadeh, B., Omarzadeh, D., Kazemi Garajeh, M., Lakes, T., & Blaschke, T. (2023). Machine learning data-driven approaches for land use/cover mapping and trend analysis using Google earth engine. Journal of Environmental Planning and Management, 66(3), 665–697. https://doi.org/10.1080/09640568.2021.2001317

Feng, Q., Gong, J., Liu, J., & Li, Y. (2015). Flood mapping based on multiple endmember spectral mixture analysis and random forest classifier—The Case of Yuyao, China. Remote Sensing, 7(9), 12539–12562. https://doi.org/10.3390/rs70912539

Ghosh, A., Sharma, R., & Joshi, P. K. (2014). Random forest classification of urban landscape using landsat archive and ancillary data: Combining seasonal maps with decision level fusion. Applied Geography, 48(March), 31–41. https://doi.org/10.1016/j.apgeog.2014.01.003

Goldblatt, R., Stuhlmacher, M. F., Tellman, B., Clinton, N., Hanson, G., Georgescu, M., Wang, C., Serrano-Candela, F., Khandelwal, A. K., Cheng, W.-H., & Balling, R. C.Jr, (2018). Using Landsat and nighttime lights for supervised pixel-based image classification of urban land cover. Remote Sensing of Environment, 205(February), 253–275. https://doi.org/10.1016/j.rse.2017.11.026

Govender, T., Dube, T., & Shoko, C. (2022). Remote sensing of land use-land cover change and climate variability on hydrological processes in Sub-Saharan Africa: Key scientific strides and challenges. Geocarto International, 37(25), 10925–10949. https://doi.org/10.1080/10106049.2022.2043451

Graesser, J., & Ramankutty, N. (2017). Detection of cropland field parcels from Landsat imagery. Remote Sensing of Environment, 201(November), 165–180. https://doi.org/10.1016/j.rse.2017.08.027

Gumma, M. K., Thenkabail, P. S., Teluguntla, P. G., Oliphant, A., Xiong, J., Giri, C., Pyla, V., Dixit, S., & Whitbread, A. M.

(2020). Agricultural cropland extent and areas of South Asia derived using Landsat Satellite 30-m time-series big-data using random forest machine learning algorithms on the Google earth engine cloud. *GIScience & Remote Sensing*, *57*(3), 302–322. https://doi.org/10.1080/15481603.2019.1690780

Hailu, A., Mammo, S., & Kidane, M. (2020). Dynamics of land use, land cover change trend and its drivers in Jimma Geneti District, Western Ethiopia. *Land Use Policy*, *99*(December), 105011. https://doi.org/10.1016/j.landusepol.2020.105011

Hassan, Z., Shabbir, R., Ahmad, S. S., Malik, A. H., Aziz, N., Butt, A., & Erum, S. (2016). Dynamics of land use and land cover change (LULCC) using geospatial techniques: A case study of Islamabad Pakistan. *SpringerPlus*, *5*(1), 812. https://doi.org/10.1186/s40064-016-2414-z

He, C., Liu, Z., Xu, M., Ma, Q., & Dou, Y. (2017). Urban expansion brought stress to food security in china: Evidence from decreased cropland net primary productivity. *The Science of the Total Environment*, *576*(January), 660–670. https://doi.org/10.1016/j.scitotenv.2016.10.107

Hobbie, R. K., & Roth, B. J. (2007). Exponential growth and decay. In *Intermediate Physics for Medicine and Biology*. 31–47. Springer New York. https://doi.org/10.1007/978-0-387-49885-0_2

Hossain, F., Kamal, M. A., & Afrin, T. (2024). Fluvio-geomorphic change of the Padma-Meghna river course using the NDWI and MNDWI techniques. *Water Science*, *38*(1), 293–310. https://doi.org/10.1080/23570008.2024.2344752

Hou, D., Meng, F., & Prishchepov, A. V. (2021). How is urbanization shaping agricultural land-use? Unraveling the Nexus between farmland abandonment and urbanization in China. *Landscape and Urban Planning*, *214*(October), 104170. https://doi.org/10.1016/j.landurbplan.2021.104170

Huete, A. R. (1988). A soil-adjusted vegetation index (SAVI). *Remote Sensing of Environment*, *25*(3), 295–309. https://doi.org/10.1016/0034-4257(88)90106-X

Hussain, S., Lu, L., Mubeen, M., Nasim, W., Karuppannan, S., Fahad, S., Tariq, A., Mousa, B. G., Mumtaz, F., & Aslam, M. (2022). Spatiotemporal variation in land use land cover in the response to local climate change using multispectral remote sensing Data. *Land*, *11*(5), 595. https://doi.org/10.3390/land11050595

Hussain, S., Raza, A., Abdo, H. G., Mubeen, M., Tariq, A., Nasim, W., Majeed, M., Almohamad, H., & Al Dughairi, A. A. (2023). Relation of land surface temperature with different vegetation indices using multi-temporal remote sensing data in Sahiwal Region, Pakistan. *Geoscience Letters*, *10*(1), 33. https://doi.org/10.1186/s40562-023-00287-6

Hütt, C., Koppe, W., Miao, Y., & Bareth, G. (2016). Best accuracy land use/land cover (LULC) classification to derive crop types using multitemporal, multisensor, and multi-polarization SAR satellite images. *Remote Sensing*, *8*(8), 684. https://doi.org/10.3390/rs8080684

Irfan, M., Razzaq, A., Chupradit, S., Javid, M., Rauf, A., & Aini Farooqi, T. J. (2022). Hydrogen production potential from agricultural biomass in Punjab Province of Pakistan. *International Journal of Hydrogen Energy*, *47*(5), 2846–2861. https://doi.org/10.1016/j.ijhydene.2021.10.257

Jafari, R., Bashari, H., & Tarkesh, M. (2017). Discriminating and monitoring rangeland condition classes with MODIS NDVI and EVI indices in Iranian Arid and Semi-Arid Lands. *Arid Land Research and Management*, *31*(1), 94–110. https://doi.org/10.1080/15324982.2016.1224955

Jozdani, S. E., Johnson, B. A., & Chen, D. (2019). Comparing deep neural networks, ensemble classifiers, and support vector machine algorithms for object-based urban land use/land cover classification. *Remote Sensing*, *11*(14), 1713. https://doi.org/10.3390/rs11141713

Kafy, A.-. A., Dey, N. N., Al Rakib, A., Rahaman, Z. A., Nasher, N. M. R., & Bhatt, A. (2021). Modeling the relationship between land use/land cover and land surface temperature in Dhaka, Bangladesh using CA-ANN algorithm. *Environmental Challenges*, *4*(August), 100190. https://doi.org/10.1016/j.envc.2021.100190

Kavhu, B., Eric Mashimbye, Z., & Luvuno, L. (2022). Characterising social-ecological drivers of landuse/cover change in a complex transboundary basin using singular or ensemble machine learning. *Remote Sensing Applications: Society and Environment*, *27*(August), 100773. https://doi.org/10.1016/j.rsase.2022.100773

Kuo, T. (2021). Identifying aging villages with primary care shortages: A geographic information system approach. *Journal of Internet Technology*, *22*(3), 615–623. doi:<https://jit.ndhu.edu.tw/article/view/2518.

Le, T. D. H., Pham, L. H., Dinh, Q. T., Hang, N. T. T., & Tran, T. A. T. (2022). Rapid method for yearly LULC classification using random forest and incorporating time-series NDVI and topography: A case study of Thanh Hoa Province, Vietnam. *Geocarto International*, *37*(27), 17200–17215. https://doi.org/10.1080/10106049.2022.2123959

Liu, J., Liu, M., Tian, H., Zhuang, D., Zhang, Z., Zhang, W., Tang, X., & Deng, X. (2005). Spatial and temporal patterns of China's Cropland during 1990–2000: An analysis based on Landsat TM Data. *Remote Sensing of Environment*, *98*(4), 442–456. https://doi.org/10.1016/j.rse.2005.08.012

Liu, Y., Meng, Q., Zhang, L., & Wu, C. (2022). NDBSI: A normalized difference bare soil index for remote sensing to improve bare soil mapping accuracy in urban and rural areas. *Catena*, *214*(July), 106265. https://doi.org/10.1016/j.catena.2022.106265

Loibl, C., Bruine de Bruin, W., Summers, B., McNair, S., & Verhallen, P. (2022). Which financial stressors are linked to food insecurity among older adults in the United Kingdom, Germany, and the Netherlands? An exploratory study. *Food Security*, *14*(2), 533–556. https://doi.org/10.1007/s12571-021-01206-3

Mananze, S., Pôças, I., & Cunha, M. (2020). Mapping and assessing the dynamics of shifting agricultural landscapes using Google earth engine cloud computing, a case study in Mozambique. *Remote Sensing*, *12*(8), 1279. https://doi.org/10.3390/rs12081279

Marzban, F., Sodoudi, S., & Preusker, R. (2018). The influence of land-cover type on the relationship between NDVI–LST and LST- T air. *International Journal of Remote Sensing*, *39*(5), 1377–1398. https://doi.org/10.1080/01431161.2017.1402386

Mikalauskiene, A., Narutaviciute-Cikanauske, R., Sarkiunaite, I., Streimikiene, D., & Zlateva, R. (2018). Social aspect of sustainable development: Issues of poverty and food shortage. *Montenegrin Journal of Economics*, *14*(2), 59–78. https://doi.org/10.14254/1800-5845/2018.14-2.4

Mjiri, I. E., Rahimi, A., & Bouasria, A. (2020). *Urban Sprawl Evolution and Soil Artificialization Assessment by Using Satellite Data from 1985 to 2019: Case of El Jadida Metropolitan in Morocco* [Paper presentation]. 2020 Second International Sustainability and Resilience Conference: Technology and Innovation in Building Designs(51154), pp. 1–5. IEEE. https://doi.org/10.1109/IEEECONF51154.2020.9319958

Mjiri, I. E., Rahimi, A., & Bouasria, A. (2022). Quantification and prediction of urban sprawl and surface temperature and assessment of their impacts on the environment: Case El Jadida (Morocco). *International Journal of Global Warming*, *26*(4), 374. https://doi.org/10.1504/IJGW.2022.122431

Mjiri, I. E., Rahimi, A., Bouasria, A., & Bounif, M. (2022 *Using RapidEye Satellite Images for the Sustainable Management of the Extension of El Jadida City (Morocco)* [Paper presentation]. 2022 International Conference on Decision Aid Sciences and Applications (DASA), pp. 761–765. IEEE. https://doi.org/10.1109/DASA54658.2022.9765099

Mottaleb, K. A., Kruseman, G., Frija, A., Sonder, K., & Lopez-Ridaura, S. (2022). Projecting wheat demand in China and India for 2030 and 2050: Implications for food security. *Frontiers in Nutrition*, *9*(January), 1077443. https://doi.org/10.3389/fnut.2022.1077443

Mountrakis, G., Im, J., & Ogole, C. (2011). Support vector machines in remote sensing: A review. *ISPRS Journal of Photogrammetry and Remote Sensing*, *66*(3), 247–259. https://doi.org/10.1016/j.isprsjprs.2010.11.001

Moura, Y. M., Galvão, L. S., dos Santos, J. R., Roberts, D. A., & Breunig, F. M. (2012). Use of MISR/terra data to study intra- and inter-annual EVI variations in the dry season of tropical forest. *Remote Sensing of Environment*, *127*(December), 260–270. https://doi.org/10.1016/j.rse.2012.09.013

Najmuddin, O., Deng, X., & Bhattacharya, R. (2018). The dynamics of land use/cover and the statistical assessment of cropland change drivers in the Kabul River Basin, Afghanistan. *Sustainability*, *10*(2), 423. https://doi.org/10.3390/su10020423

Odey, G., Adelodun, B., Lee, S., Adeyemi, K. A., & Choi, K. S. (2023). Assessing the impact of food trade centric on land, water, and food security in South Korea. *Journal of Environmental Management*, *332*(April), 117319. https://doi.org/10.1016/j.jenvman.2023.117319

Odhiambo, V. O., Hendriks, S. L., & Mutsvangwa-Sammie, E. P. (2021). The effect of an objective weighting of the global food security index's natural resources and resilience component on country scores and ranking. *Food Security*, *13*(6), 1343–1357. https://doi.org/10.1007/s12571-021-01176-6

Olanrewaju, S. O., Olafioye, S. O., & Oguntade, E. S. (2020). Modelling Nigeria population growth: A trend analysis approach. *International Journal of Innovative Science and Research Technology*, *5*(4), 997–1017. www.ijisrt.com

Orhan, O., & Yakar, M. (2016). Investigating land surface temperature changes using Landsat data in Konya, Turkey. *The International Archives of the Photogrammetry, Remote Sensing and Spatial Information Sciences*, *XLI-B8*(June), 285–289. https://doi.org/10.5194/isprs-archives-XLI-B8-285-2016

Pal, M. (2008). Ensemble of support vector machines for land cover classification. *International Journal of Remote Sensing*, *29*(10), 3043–3049. https://doi.org/10.1080/01431160802007624

Pal, S., & Ziaul, S. (2017). Detection of land use and land cover change and land surface temperature in English bazar urban centre. *The Egyptian Journal of Remote Sensing and Space Science*, *20*(1), 125–145. https://doi.org/10.1016/j.ejrs.2016.11.003

Pandey, B., & Seto, K. C. (2015). Urbanization and agricultural land loss in India: Comparing satellite estimates with census data. *Journal of Environmental Management*, *148*(January), 53–66. https://doi.org/10.1016/j.jenvman.2014.05.014

Patel, S. K., Verma, P., & Shankar Singh, G. (2019). Agricultural growth and land use land cover change in peri-urban India. *Environmental Monitoring and Assessment*, *191*(9), 600. https://doi.org/10.1007/s10661-019-7736-1

Pittman, K., Hansen, M. C., Becker-Reshef, I., Potapov, P. V., & Justice, C. O. (2010). Estimating global cropland extent with multi-year MODIS data. *Remote Sensing*, *2*(7), 1844–1863. https://doi.org/10.3390/rs2071844

Piyoosh, A. K., & Ghosh, S. K. (2018). Development of a modified bare soil and urban index for Landsat 8 satellite data. *Geocarto International*, *33*(4), 423–442. https://doi.org/10.1080/10106049.2016.1273401

Popescu, G. C., & Popescu, M. (2022). COVID-19 pandemic and agriculture in Romania: Effects on agricultural systems, compliance with restrictions and relations with authorities. *Food Security*, *14*(2), 557–567. https://doi.org/10.1007/s12571-021-01239-8

Qadri, S. M. T., Hamdan, A., Raj, V., Ehsan, M., Shamsuddin, N., Hakimi, M. H., & Mustapha, K. A. (2023). Assessment of land surface temperature from the Indian cities of Ranchi and Dhanbad during COVID-19 Lockdown: Implications on the urban climatology. *Sustainability*, *15*(17), 12961. https://doi.org/10.3390/su151712961

Rahimi, A., El Mjiri, I., Bouasria, A., & Zaakour, F. (2022 *Applying Machine Learning to the Study of Environmental Dynamics and Sustainable Management of the Argan Grove in the El Guerdane Region (Souss Plain, Morocco)* [Paper presentation]. 2022 International Conference on Decision Aid Sciences and Applications (DASA), In 766–770. IEEE. https://doi.org/10.1109/DASA54658.2022.9765214

Rahimi, A., Khalil, Z., Bouasria, A., El Mjiri, I., & Bounif, M. (2021). Land surface temperature responses to land use land cover dynamics (District of Taroudant, Morocco). " *The 1st International Electronic Conference on Agronomy*, 28. https://doi.org/10.3390/IECAG2021-09726

Rana, V. K., & Venkata Suryanarayana, T. M. (2020). Performance evaluation of MLE, RF and SVM classification algorithms for watershed scale land use/land cover mapping using sentinel 2 bands. *Remote Sensing Applications: Society and Environment*, *19*(August), 100351. https://doi.org/10.1016/j.rsase.2020.100351

Raza, D., Khushi, M., Shu, H., Aslam, H., Saleem, M. S., Ahmad, A., Mirza, S., Saeed, U., & Khan, S. U. (2024). CA-ANN based LULC prediction and influence assessment on LST-NDVI using multi-temporal satellite images. *Environmental Earth Sciences*, *83*(5), 144. https://doi.org/10.1007/s12665-024-11467-8

Raza, D., Shu, H., Khan, S. U., Ehsan, M., Saeed, U., Aslam, H., Aslam, R. W., & Arshad, M. (2022). Comparative geospatial approach for agricultural crops identification in inter-fluvial plain-A case study of Sahiwal District, Pakistan. *Pakistan Journal of Agricultural Sciences*, *59*(4), 567–578. https://doi.org/10.21162/PAKJAS/22.127

Raza, D., Shu, H., Nazeer, M., Aslam, H., Mirza, S., Xiao, X., Sardar, A., & Aeman, H. (2024). Improved method for cropland extraction of seasonal crops from multi-sensor satellite data. *International Journal of Remote Sensing*, *45*(18), 6249–6284. https://doi.org/10.1080/01431161.2024.2388864

Rouse, J. W., Hass, R. H., Schell, J. A., & Deering, D. W. (1973). Monitoring vegetation systems in the Great Plains with ERTS. In *The Third ERTS Symposium. NASA SP-351*, 309—317. https://ntrs.nasa.gov/citations/19740022614

Sagan, V., Peterson, K. T., Maimaitijiang, M., Sidike, P., Sloan, J., Greeling, B. A., Maalouf, S., & Adams, C. (2020). Monitoring inland water quality using remote sensing: Potential and limitations of spectral indices, bio-optical simulations, machine learning, and cloud computing. *Earth-Science Reviews*, *205*(June), 103187. https://doi.org/10.1016/j.earscirev.2020.103187

Sajan, B., Mishra, V. N., Kanga, S., Meraj, G., Kumar Singh, S., & Kumar, P. (2022). Cellular automata-based artificial neural network model for assessing past, present, and future land use/land cover dynamics. *Agronomy*, *12*(11), 2772. https://doi.org/10.3390/agronomy12112772

Sharma, R., Hara, K., & Tateishi, R. (2017). High-resolution vegetation mapping in Japan by combining Sentinel-2 and Landsat 8 based multi-temporal datasets through machine learning and cross-validation approach. *Land*, *6*(3), 50. https://doi.org/10.3390/land6030050

Shi, Y., Qi, Z., Liu, X., Niu, N., & Zhang, H. (2019). Urban land use and land cover classification using multisource remote sensing images and social media data. *Remote Sensing*, *11*(22), 2719. https://doi.org/10.3390/rs11222719

Shih, H-c., Stow, D. A., & Tsai, Y. H. (2019). Guidance on and comparison of machine learning classifiers for Landsat-based land cover and land use mapping. *International Journal of Remote Sensing*, *40*(4), 1248–1274. https://doi.org/10.1080/01431161.2018.1524179

Shirzad, H., Barati, A. A., Ehteshammajd, S., Goli, I., Siamian, N., Moghaddam, S. M., Pour, M., Tan, R., Janečková, K., Sklenička, P., & Azadi, H. (2022). Agricultural land tenure system in Iran: An overview. *Land Use Policy*, *123*(December), 106375. https://doi.org/10.1016/j.landusepol.2022.106375

Skakun, S., Kussul, N., Shelestov, A. Y., Lavreniuk, M., & Kussul, O. (2016). Efficiency assessment of multitemporal C-Band Radarsat-2 intensity and Landsat-8 surface reflectance satellite imagery for crop classification in Ukraine. *IEEE Journal of Selected Topics in Applied Earth Observations and Remote Sensing*, *9*(8), 3712–3719. https://doi.org/10.1109/JSTARS.2015.2454297

Sobrino, J. A., Jiménez-Muñoz, J. C., & Paolini, L. (2004). Land surface temperature retrieval from LANDSAT TM 5. *Remote Sensing of Environment*, *90*(4), 434–440. https://doi.org/10.1016/j.rse.2004.02.003

Sobrino, J. A., Jimenez-Munoz, J. C., Soria, G., Romaguera, M., Guanter, L., Moreno, J., Plaza, A., & Martinez, P. (2008). Land surface emissivity retrieval from different VNIR and TIR sensors. *IEEE Transactions on Geoscience and Remote Sensing*, *46*(2), 316–327. https://doi.org/10.1109/TGRS.2007.904834

Sohail, M. T., Manzoor, Z., Ehsan, M., Al-Ansari, N., Khan, M. B., Shafi, A., Ullah, J., Hussain, A., Raza, D., Usman, U., Akbar, S., & Elbeltagi, A. (2023). Impacts of urbanization, LULC, LST, and NDVI changes on the static water table with possible solutions and water policy discussions: A case from Islamabad, Pakistan. *Frontiers in Environmental Science*, *11*(February). https://doi.org/10.3389/fenvs.2023.1018500

Su, S., Ma, X., & Xiao, R. (2014). Agricultural landscape pattern changes in response to urbanization at Ecoregional Scale. *Ecological Indicators*, *40*(May), 10–18. https://doi.org/10.1016/j.ecolind.2013.12.013

Sun, L., Gao, F., Xie, D., Anderson, M., Chen, R., Yang, Y., Yang, Y., & Chen, Z. (2021). Reconstructing daily 30 m NDVI over complex agricultural landscapes using a crop reference curve approach. *Remote Sensing of Environment*, *253*(February), 112156. https://doi.org/10.1016/j.rse.2020.112156

Sun, Z., Wang, G., Li, P., Wang, H., Zhang, M., & Liang, X. (2024). An improved random forest based on the classification accuracy and correlation measurement of decision trees. *Expert Systems with Applications*, *237*(March), 121549. https://doi.org/10.1016/j.eswa.2023.121549

Tahir, M., & Khaliq, T. (2018). 2 Land use in Pakistan. *Developing Sustainable Agriculture in Pakistan*. CRC Press.

Tao, Z., Cheng, Y., & Liu, J. (2020). Hierarchical two-step floating catchment area (2SFCA) method: Measuring the spatial accessibility to hierarchical healthcare facilities in Shenzhen, China. *International Journal for Equity in Health*, *19*(1), 164. https://doi.org/10.1186/s12939-020-01280-7

Tariq, A., Yan, J., Gagnon, A. S., Riaz Khan, M., & Mumtaz, F. (2023). Mapping of cropland, cropping patterns and crop types by combining optical remote sensing images with decision tree classifier and random forest. *Geo-Spatial Information Science*, *26*(3), 302–320. https://doi.org/10.1080/10095020.2022.2100287

Tu, Y., Chen, B., Yu, L., Xin, Q., Gong, P., & Xu, B. (2021). How does urban expansion interact with cropland loss? A comparison of 14 Chinese cities from 1980 to 2015. *Landscape Ecology*, *36*(1), 243–263. https://doi.org/10.1007/s10980-020-01137-y

Ullah, S., Ahmad, K., Umer Sajjad, R., Abbasi, A. M., Nazeer, A., & Ahmad Tahir, A. (2019). Analysis and simulation of land cover changes and their impacts on land surface temperature in a lower Himalayan Region. *Journal of Environmental Management*, *245*(September), 348–357. https://doi.org/10.1016/j.jenvman.2019.05.063

United Nation. (2017). *Sustainable Development Goals Report 2017 - Zero Hunger*. https://unstats.un.org/sdgs/report/2017/

United Nation. (2023). *Sustainable Development Goals Report 2023: Goal 02*. https://unstats.un.org/sdgs/report/2023/Goal-02/

USDA. (2015). *Pakistan Gain and Feed Annual. Foreign Agriculture Services*. https://apps.fas.usda.gov/newgainapi/api/report/downloadreportbyfilename?filename=Grain and Feed Annual_Islamabad_Pakistan_4-3-2015.pdf.

Valle, D., Izbicki, R., & Vieira Leite, R. (2023). Quantifying uncertainty in land-use land-cover classification using conformal statistics. *Remote Sensing of Environment*, *295*(September), 113682. https://doi.org/10.1016/j.rse.2023.113682

Vivekananda, G. N., Swathi, R., & Sujith, A. V. L. N. (2021). Multi-temporal image analysis for LULC classification and change detection. *European Journal of Remote Sensing*, *54*(sup2), 189–199. https://doi.org/10.1080/22797254.2020.1771215

Vogels, M. F. A., de Jong, S. M., Sterk, G., & Addink, E. A. (2017). Agricultural cropland mapping using black-and-white aerial photography, object-based image analysis and random forests. *International Journal of Applied Earth Observation and Geoinformation*, 54(February), 114–123. https://doi.org/10.1016/j.jag.2016.09.003

Wang, J., Bretz, M., Dewan, M. A. A., & Delavar, M. A. (2022). Machine learning in modelling land-use and land cover-change (LULCC): Current status, challenges and prospects. *The Science of the Total Environment*, 822(May), 153559. https://doi.org/10.1016/j.scitotenv.2022.153559

Wang, J., Wu, Z., Wu, C., Cao, Z., Fan, W., & Tarolli, P. (2018). Improving impervious surface Estimation: An integrated method of classification and regression trees (CART) and linear spectral mixture analysis (LSMA) based on error analysis. *GIScience & Remote Sensing*, 55(4), 583–603. https://doi.org/10.1080/15481603.2017.1417690

Wang, J., Zhao, Y., Li, C., Yu, L., Liu, D., & Gong, P. (2015). Mapping global land cover in 2001 and 2010 with spatial-temporal consistency at 250m resolution. *ISPRS Journal of Photogrammetry and Remote Sensing*, 103(May), 38–47. https://doi.org/10.1016/j.isprsjprs.2014.03.007

Wang, Y., Fang, Z., Hong, H., Costache, R., & Tang, X. (2021). Flood susceptibility mapping by integrating frequency ratio and index of entropy with multilayer perceptron and classification and regression tree. *Journal of Environmental Management*, 289(July), 112449. https://doi.org/10.1016/j.jenvman.2021.112449

Wu, Y., Zhang, P., Li, J., & Hou, J. (2022). Spatial distribution evolution and optimization path of eco-efficiency of cultivated land use: A case study of Hubei Province, China. *Sustainability*, 14(18), 11417. https://doi.org/10.3390/su141811417

Wulder, M. A., Loveland, T. R., Roy, D. P., Crawford, C. J., Masek, J. G., Woodcock, C. E., Allen, R. G., Anderson, M. C., Belward, A. S., Cohen, W. B., Dwyer, J., Erb, A., Gao, F., Griffiths, P., Helder, D., Hermosilla, T., Hipple, J. D., Hostert, P., Hughes, M. J., … Zhu, Z. (2019). Current status of Landsat program, science, and applications. *Remote Sensing of Environment*, 225(May), 127–147. https://doi.org/10.1016/j.rse.2019.02.015

Würtenberger, L., Koellner, T., & Binder, C. R. (2006). Virtual land use and agricultural trade: Estimating environmental and socio-economic impacts. *Ecological Economics*, 57(4), 679–697. https://doi.org/10.1016/j.ecolecon.2005.06.004

Xu, H. (2006). Modification of normalised difference water index (NDWI) to enhance open water features in remotely sensed imagery. *International Journal of Remote Sensing*, 27(14), 3025–3033. https://doi.org/10.1080/01431160600589179

Xu, Z., Yu, Z., & Zhao, J. (2013). Theory and application for the promotion of wheat production in China: Past, present and future. *Journal of the Science of Food and Agriculture*, 93(10), 2339–2350. https://doi.org/10.1002/jsfa.6098

Yang, C., Huang, Q., Li, Z., Liu, K., & Hu, F. (2017). Big data and cloud computing: innovation opportunities and challenges. *International Journal of Digital Earth*, 10(1), 13–53. https://doi.org/10.1080/17538947.2016.1239771

Yang, G., Yu, W., Yao, X., Zheng, H., Cao, Q., Zhu, Y., Cao, W., & Cheng, T. (2021). AGTOC: A novel approach to winter wheat mapping by automatic generation of training samples and one-class classification on Google Earth Engine. *International Journal of Applied Earth Observation and Geoinformation*, 102(October), 102446. https://doi.org/10.1016/j.jag.2021.102446

Yang, S., Xu, W., Xie, Y., Sohail, M. T., & Gong, Y. (2023). Impact of natural hazards on agricultural production decision making of peasant households: On the basis of the micro survey Data of Hunan Province. *Sustainability*, 15(6), 5336. https://doi.org/10.3390/su15065336

Zahoor, Z., Latif, M. I., Khan, I., & Hou, F. (2022). "Abundance of natural resources and environmental sustainability: The roles of manufacturing value-added, urbanization, and permanent cropland." *Environmental Science and Pollution Research International*, 29(54), 82365–82378. https://doi.org/10.1007/s11356-022-21545-8

Zambrano, F., Vrieling, A., Nelson, A., Meroni, M., & Tadesse, T. (2018). Prediction of drought-induced reduction of agricultural productivity in chile from MODIS, rainfall estimates, and climate oscillation indices. *Remote Sensing of Environment*, 219(December), 15–30. https://doi.org/10.1016/j.rse.2018.10.006

Zeng, L., Zhang, Q., Ding, J., Feng, Q., & Wu, F. (2023). Re-coupling crop and livestock through spatial analysis and site selection of manure transfer hubs for sustainable agriculture. *Agronomy for Sustainable Development*, 43(5), 68. https://doi.org/10.1007/s13593-023-00921-9

Zewude, A., Govindu, V., Shibru, S., & Woldu, Z. (2022). Assessment of spatiotemporal dynamics of land and vegetation cover change detection in maze national park, Southwest Ethiopia. *Environmental Monitoring and Assessment*, 194(7), 460. https://doi.org/10.1007/s10661-022-10039-2

Zhang, C., Wei, S., Ji, S., & Lu, M. (2019). Detecting large-scale urban land cover changes from very high resolution remote sensing images using CNN-based classification. *ISPRS International Journal of Geo-Information*, 8(4), 189. https://doi.org/10.3390/ijgi8040189

Zhang, F., & Yang, X. (2020). Improving land cover classification in an urbanized coastal area by random forests: The role of variable selection. *Remote Sensing of Environment*, 251(December), 112105. https://doi.org/10.1016/j.rse.2020.112105

Zhang, Q., Qu, Y., & Zhan, L. (2023). Great transition and new pattern: agriculture and rural area green development and its coordinated relationship with economic growth in China. *Journal of Environmental Management*, 344(October), 118563. https://doi.org/10.1016/j.jenvman.2023.118563

Zhang, X. Q. (2016). The trends, promises and challenges of urbanisation in the World. *Habitat International*, 54(May), 241–252. https://doi.org/10.1016/j.habitatint.2015.11.018

Zhang, X., Liu, L., Wu, C., Chen, X., Gao, Y., Xie, S., & Zhang, B. (2020). Development of a global 30 m impervious surface map using multisource and multitemporal remote sensing datasets with the Google earth engine platform. *Earth System Science Data*, 12(3), 1625–1648. https://doi.org/10.5194/essd-12-1625-2020

Zhang, X-w., Liu, J-f., Qin, Z., & Qin, F. (2019). Winter wheat identification by integrating spectral and temporal information derived from multi-resolution remote sensing data. *Journal of Integrative Agriculture*, 18(11), 2628–2643. https://doi.org/10.1016/S2095-3119(19)62615-8

Zhang, Z., Du, J., Shen, Z., El Asraoui, H., & Song, M. (2024). Effects of modern agricultural demonstration zones on cropland utilization efficiency: An Empirical study based on county pilot. *Journal of Environmental Management*, *349*(January), 119530. https://doi.org/10.1016/j.jenvman.2023.119530

Zhao, Z., Islam, F., Waseem, L. A., Tariq, A., Nawaz, M., Islam, I. U., Bibi, T., Rehman, N. U., Ahmad, W., Aslam, R. W., Raza, D., & Hatamleh, W. A. (2024). Comparison of three machine learning algorithms using Google Earth Engine for land use land cover classification. *Rangeland Ecology & Management*, *92*(January), 129–137. https://doi.org/10.1016/j.rama.2023.10.007

Zhong, H., Liu, Z., & Wang, J. (2022). Understanding impacts of cropland pattern dynamics on grain production in China: An integrated analysis by fusing statistical data and satellite-observed data. *Journal of Environmental Management*, *313*(July), 114988. https://doi.org/10.1016/j.jenvman.2022.114988

Zhu, J., Yin, Y., Lu, J., Warner, T. A., Xu, X., Lyu, M., Wang, X., Guo, C., Cheng, T., Zhu, Y., Cao, W., Yao, X., Zhang, Y., & Liu, L. (2023). The relationship between wheat yield and sun-induced chlorophyll fluorescence from continuous measurements over the growing season. *Remote Sensing of Environment*, *298*(December), 113791. https://doi.org/10.1016/j.rse.2023.113791